

BF₃-mediated C-H/C-Li coupling of 1,3,7-triazapyrene with 2-thienyllithium in the design of push-pull fluorophores and chemosensors for nitroaromatics

**Igor A. Lavrinchenko,^a Timofey D. Moseev,^a Mikhail V. Varaksin,^{a,b*}
Grigoriy V. Zyryanov,^{a,b} Olga S. Taniya,^a Anton N. Tsmokalyuk,^a
Oleg P. Demidov,^c Ivan V. Borovlev,^c Valery N. Charushin,^{a,b} Oleg N. Chupakhin,^{a,b*}**

^a *Ural Federal University, 19 Mira Str., 620002 Ekaterinburg, Russia*

^b *Institute of Organic Synthesis, Ural Branch of the Russian Academy of Sciences, 22 S.
Kovalevskaya Str., 620990 Ekaterinburg, Russia*

^c *North Caucasus Federal University, 355009, Stavropol, Russia*

E-mail: m.v.varaksin@urfu.ru

E-mail: chupakhin@ios.uran.ru

Table of contents

1. Copies of the NMR spectra.....	S2
2. Optical studies	S5
2.1. Absorbance spectra of compound 3a,b.....	S5
2.2. Lippert-Mataga plot of compound 3a,b	S6
2.3. Lifetime measurement	S7
3. Nitroaromatics detection spectra	S8
3.1. Absorption spectra of nitroaromatics.....	S8
3.2. Stern-Volmer calculations	S8
3.3. Quenching mechanism.....	S9
3.4. Perrin calculation	S10
3.5. Stern-Volmer, Perrin, and LOD graphs for compound 3a	S10
4. DFT calculations.....	S25
5. Molecular orbitals images	S27
6. The molecular electronic potential diagrams	S30
References	S32

1. Copies of the NMR spectra

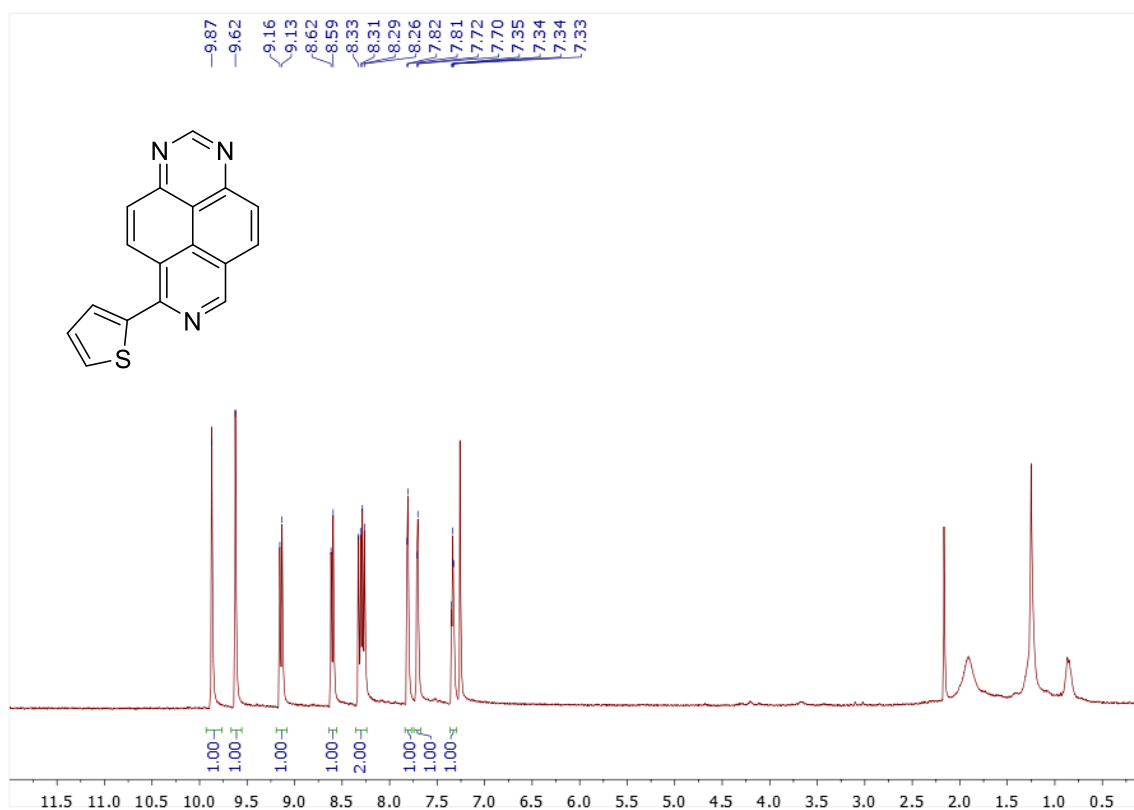


Figure S1. ¹H NMR spectrum of compound **3a** in DCCl₃ (400 MHz) at 298 K

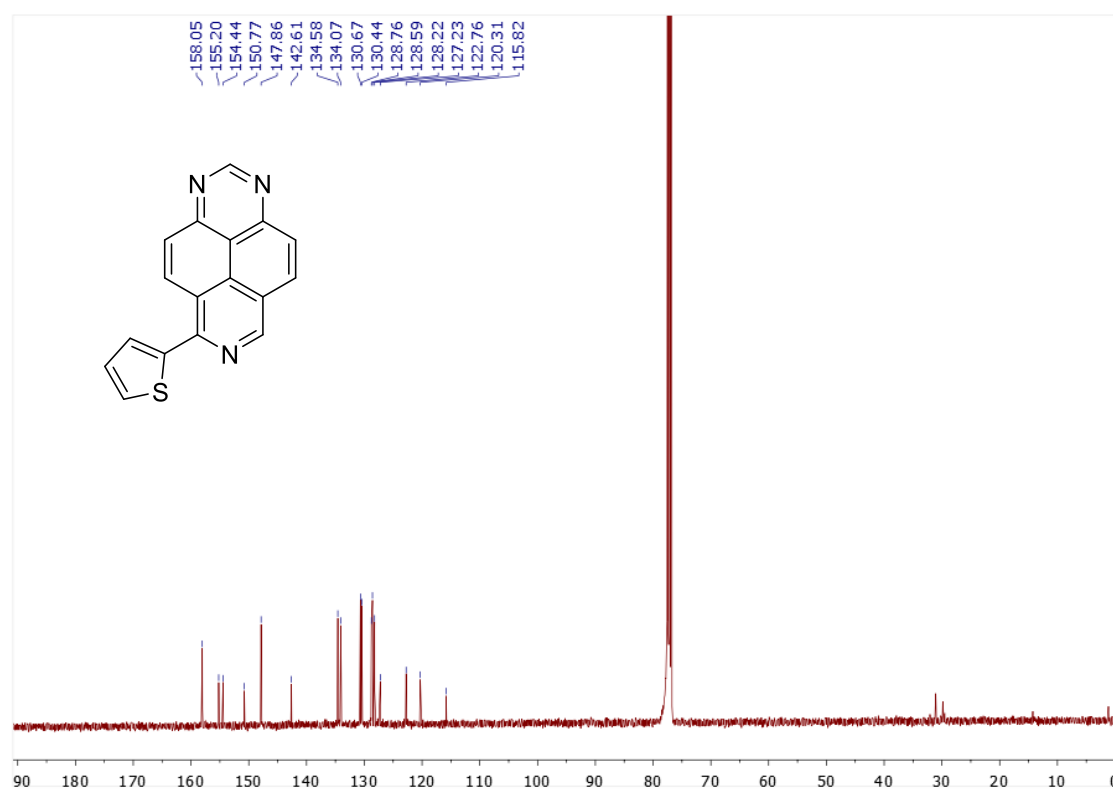


Figure S2. ¹³C NMR spectrum of compound **3a** in DCCl₃ (101 MHz) at 298 K

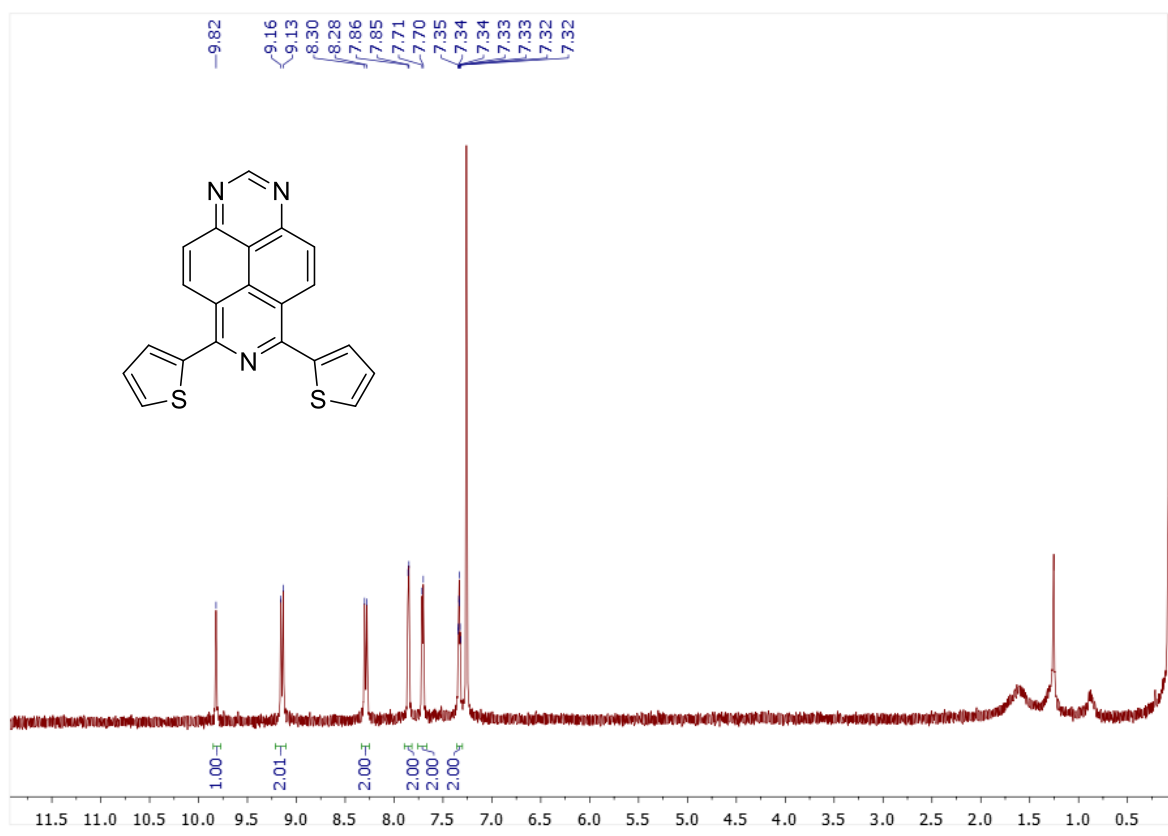


Figure S3. ^1H NMR spectrum of compound **3b** in DCCl_3 (400 MHz) at 298 K

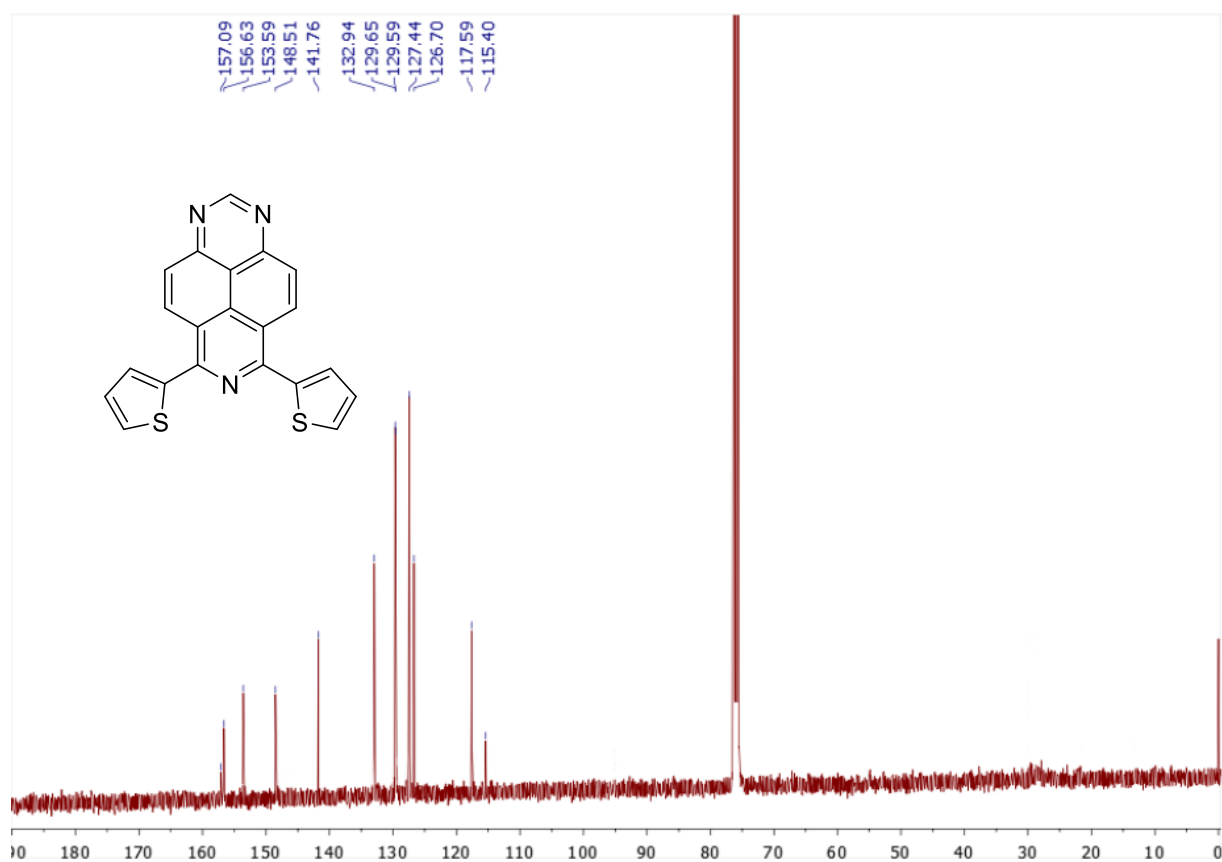


Figure S4. ^{13}C NMR spectrum of compound **3b** in DCCl_3 (101 MHz) at 298 K

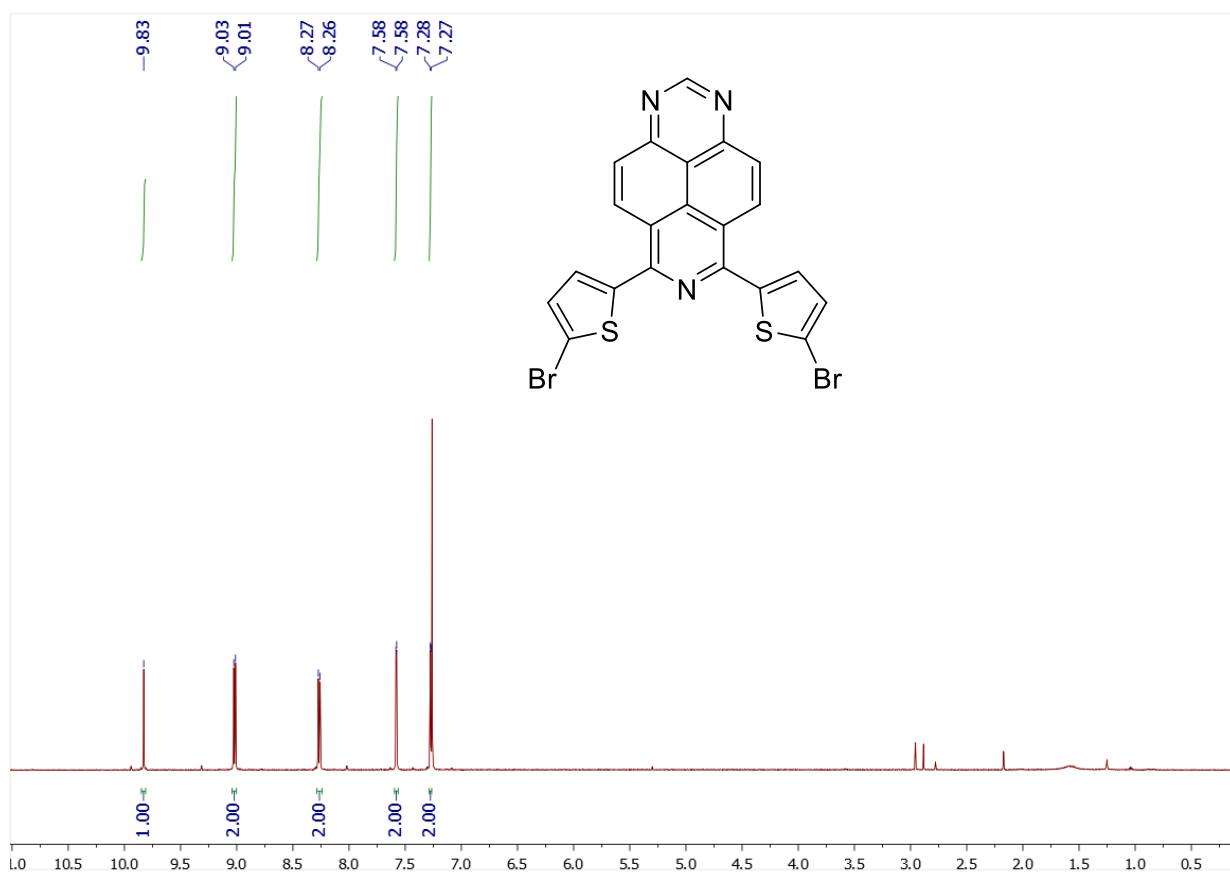


Figure S5. ^1H NMR spectrum of compound **4** in DCCl_3 (600 MHz) at 298 K

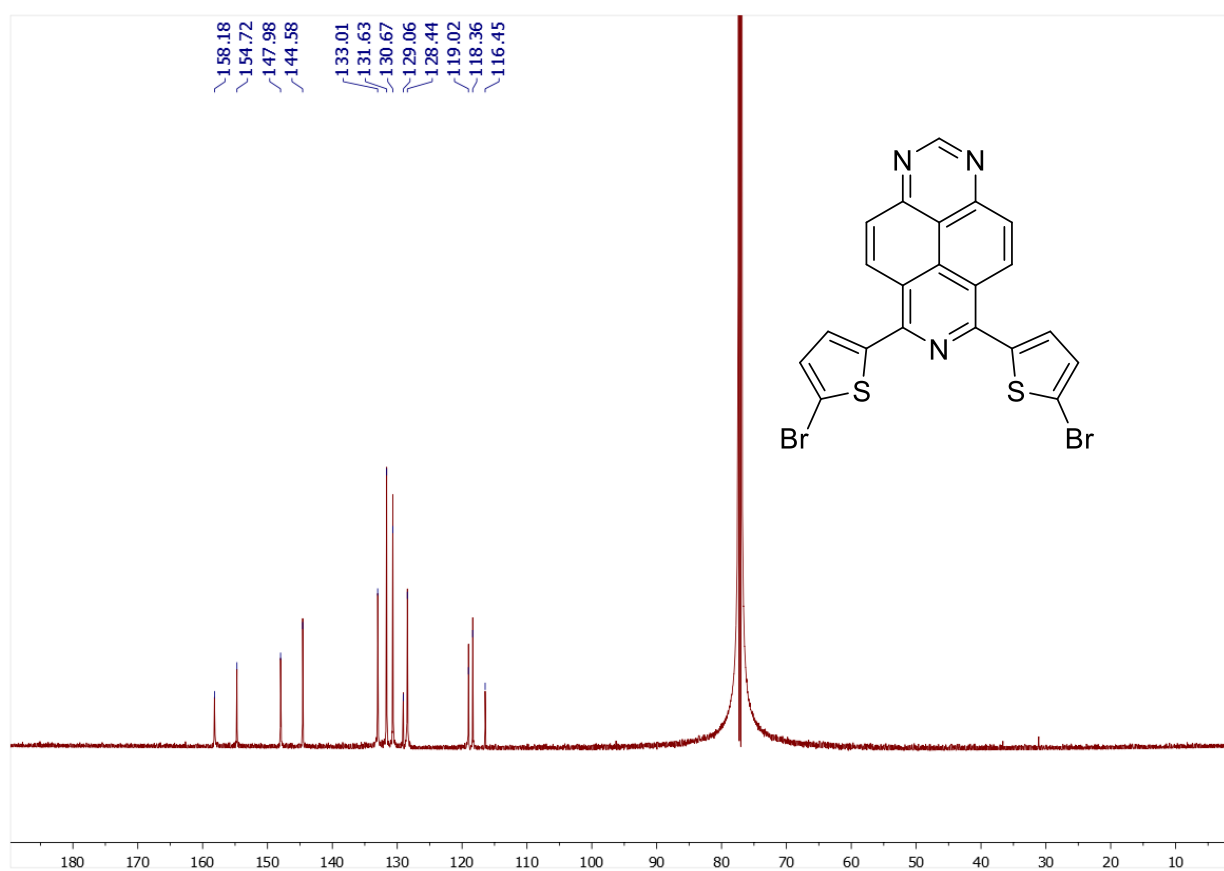


Figure S6. ^{13}C NMR spectrum of compound **4** in DCCl_3 (151 MHz) at 298 K

2. Optical studies

2.1. Absorbance spectra of compound 3a,b

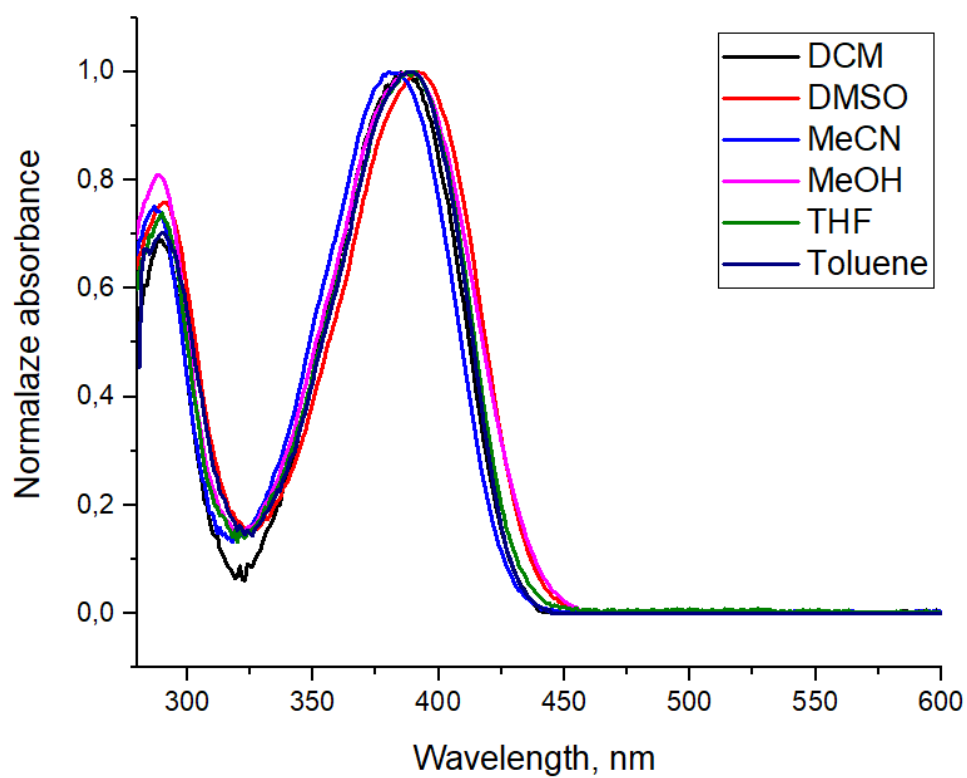


Figure S7. Normalized absorbance spectra of **3a**

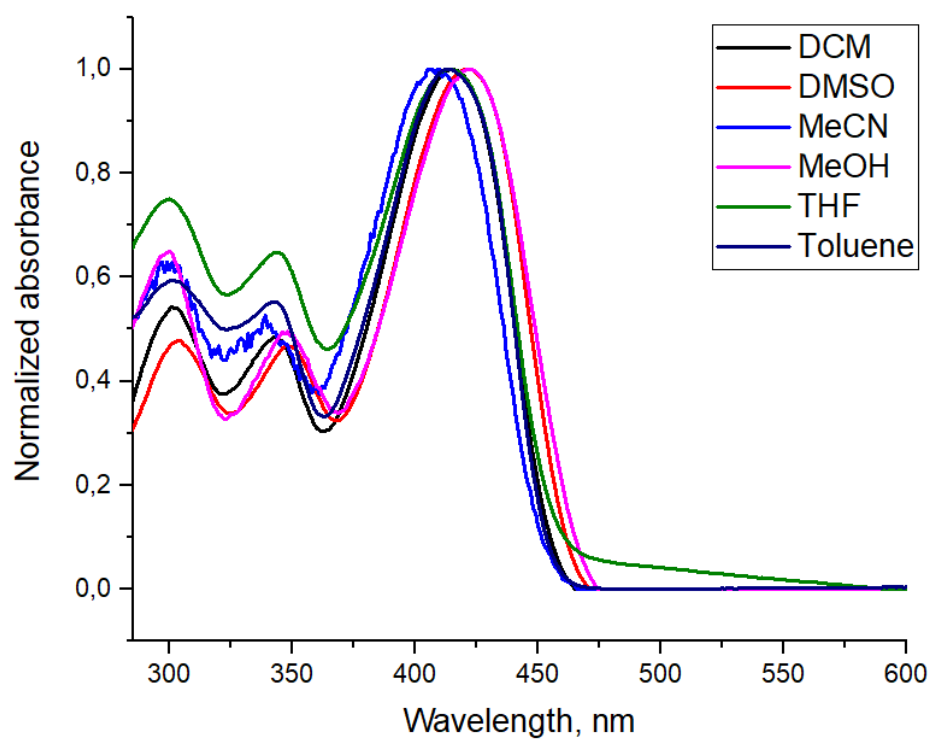


Figure S8. Normalized absorbance spectra of **3b**

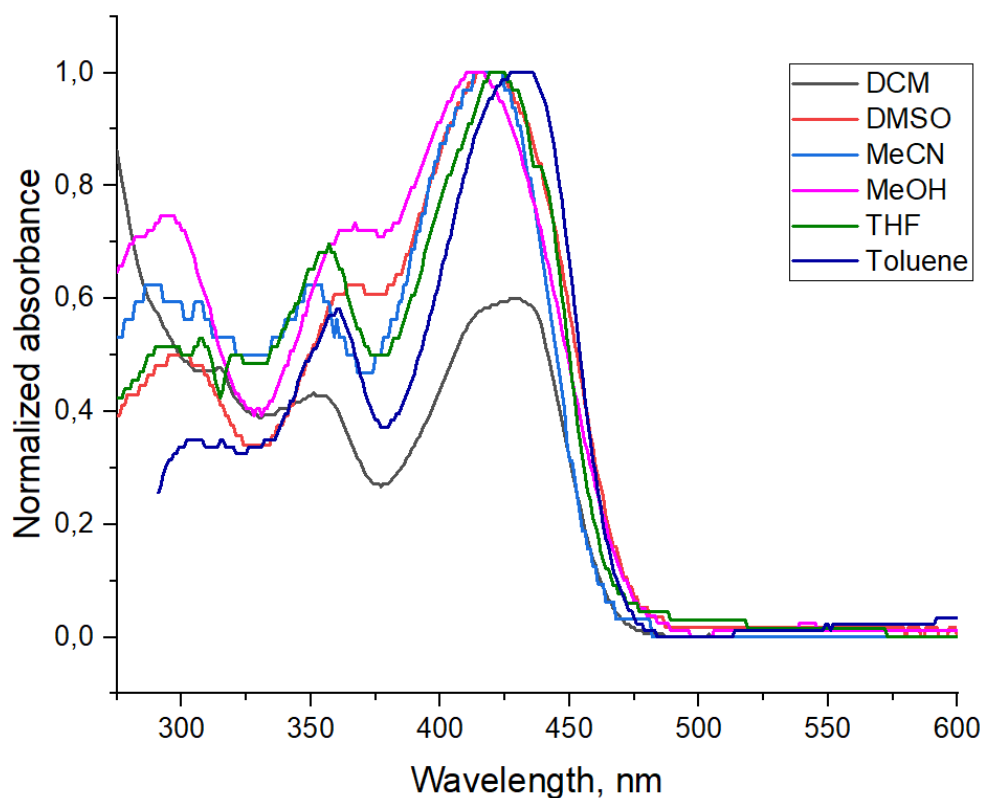


Figure S9. Normalized absorbance spectra of **4**

2.2. Lippert-Mataga plot of compound **3a,b**

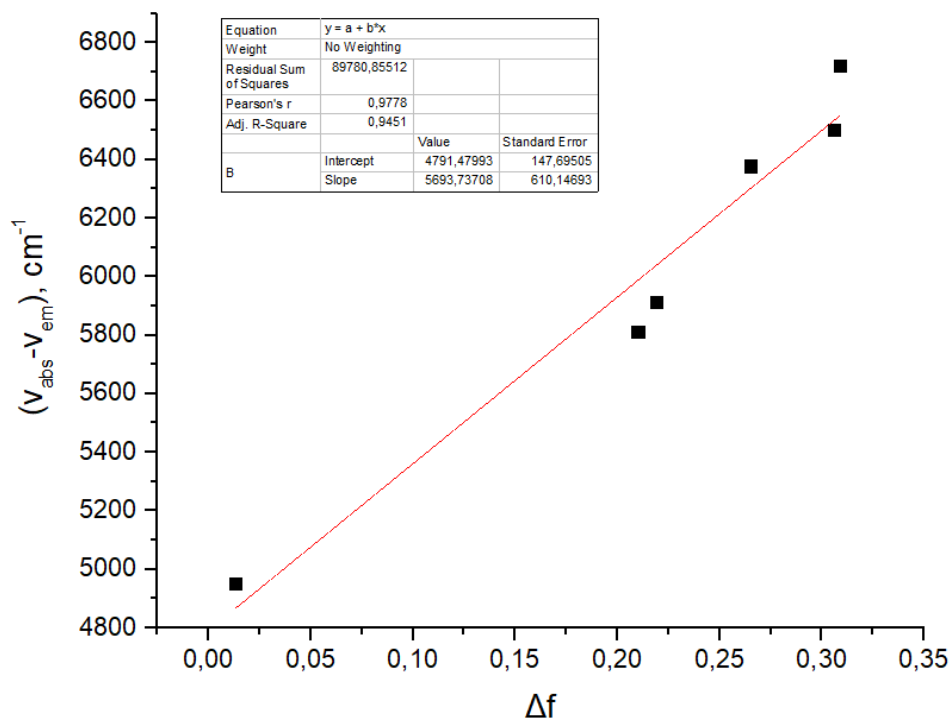


Figure S10. Lippert-Mataga plot of compound **3a**

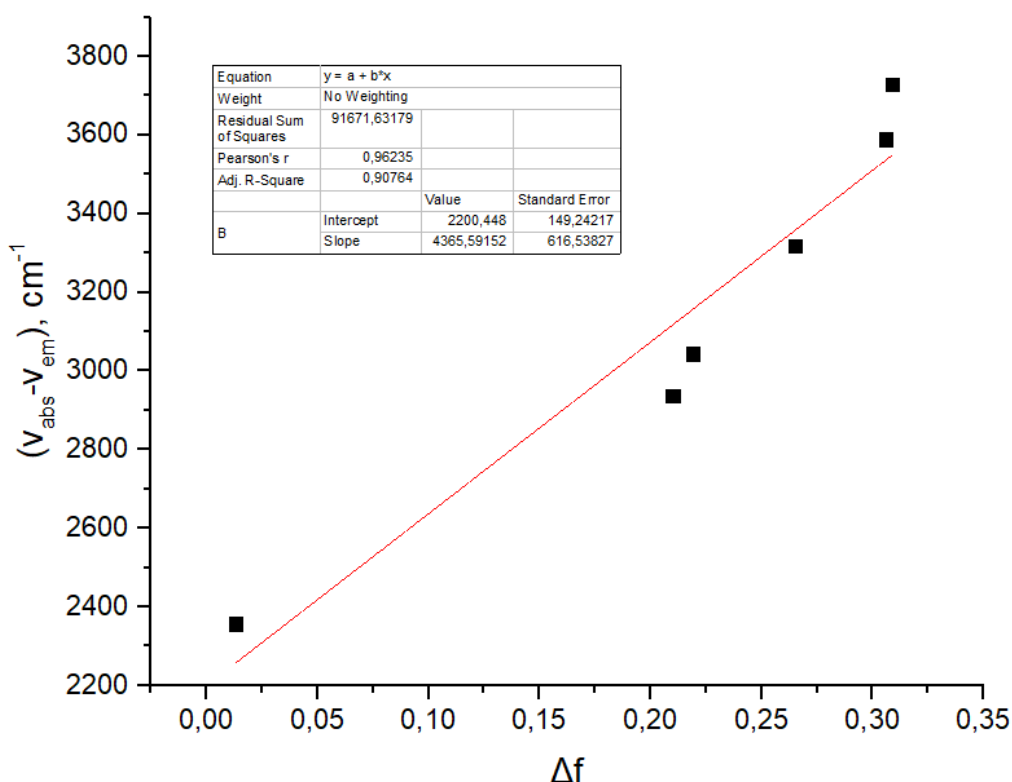


Figure S11. Lippert-Mataga plot of compound **3b**

2.3. Lifetime measurement

Fluorescence decay parameters for compounds **3a,b** are $\lambda_{\text{ex}} = 370$ nm, the decay times (τ_1 , τ_2 , and τ_3), the respective fractional contributions (α_1 , α_2 and α_3), the weighted average decay time (τ_{av}) and the quality of fitting (χ^2) are shown in Table 1.

When studying the effect of substituents on the luminescence lifetime, it was found that the lifetime of both compounds is ~ 1.5 ns. Thus, the presence of the second donor substituent in 1,3,7-triazapyrene moiety does not increase the fluorescence lifetime.

Table S1. Lifetime measurement of compounds **3a,b**

Compound	τ_1 (ns) ^a	α_1 ^b	τ_2 (ns) ^a	α_2 ^b	τ_3 (ns) ^a	α_3 ^b	τ_{av} ^c (ns)	χ^2 ^d
3a	0.39	34.79	0.39	-34.63	1.64	0.84	1.58	1.12
3b	0.5	0.07	1.58	0.93	-	-	1.50	0.94

a: Decay time; b: Fractional contribution; c: Weighted average decay time $\tau_{\text{av}} = \sum (\tau_i \times \alpha_i)$; d: Quality of fitting

3. Nitroaromatics detection spectra

3.1. Absorption spectra of nitroaromatics

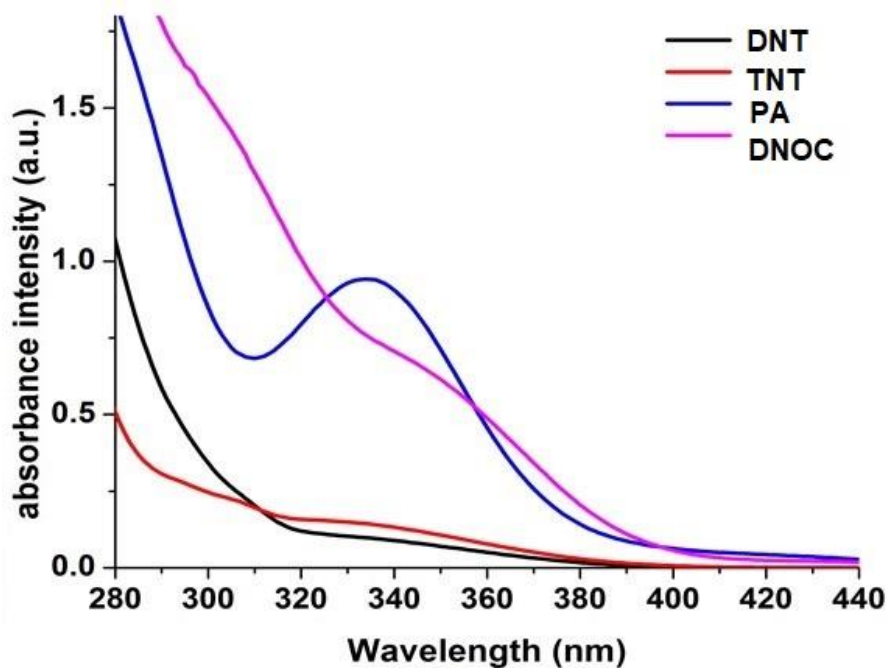


Figure S12. Absorption spectra of nitroaromatic analytes. Sample preparation: $C = 10^{-5}$ M in MeCN

3.2. Stern-Volmer calculations

The Stern-Volmer quenching model show the dependence of the change in the emission intensity on the analyte concentration is determined.

$$I_0/I = 1 + K_{sv} [Q]$$

The coupling constant for the Stern-Volmer equation was calculated as the tangent of the slope of the dependence plot $((I_0/I)-1)$ on the concentration of the quencher ($[Q]$). The analyte concentration $[Q]$ was recalculated using the formula: $[Q] = (C_q \times V_q)/(V_q+3E-3)$.

3.3. Quenching mechanism

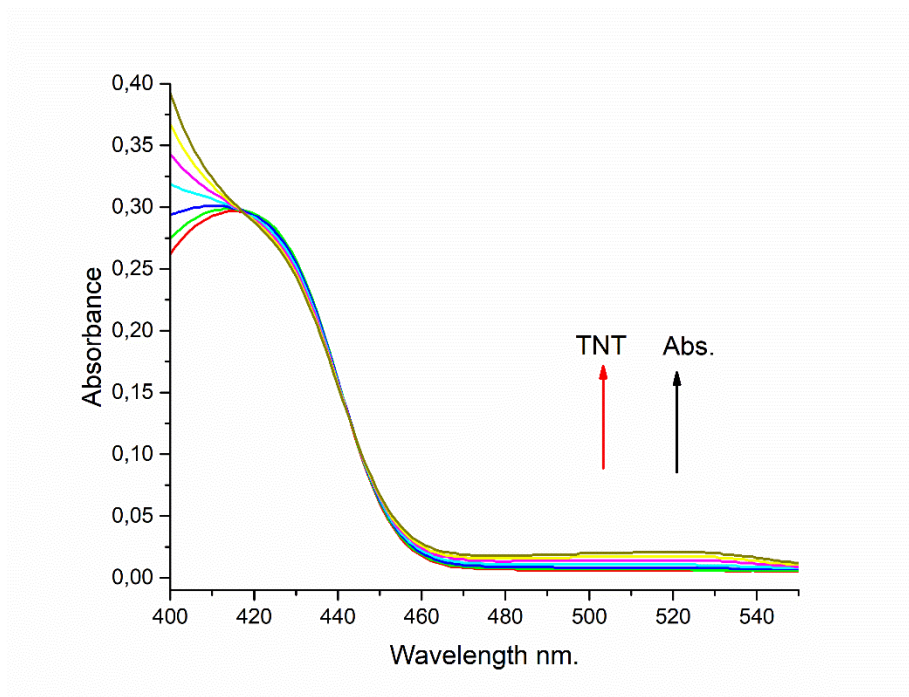


Figure S13. Experiments on quenching the absorption of the sensor **3b** ($C = 10^{-6}$ M) with a solution of TNT ($C = 2 \times 10^{-5}$ M)

Table S2. Lifetime measurement of compound **3b** ($C = 10^{-6}$ M) upon addition of TNT ($C = 2 \times 10^{-4}$ M)

N_0	TNT (μM)	τ_1 (ns) ^a	α_1 ^b	τ_2 (ns) ^a	α_2 ^b	τ_{av} (ns) ^c	χ^2 ^d
1	0	1.06	0.72	1.86	0.28	1.28	1.04
2	0.7	1.07	0.74	1.88	0.26	1.28	1.10
3	1.3	1.04	0.68	1.80	0.32	1.28	1.09
4	1.98	1.06	0.75	1.93	0.25	1.27	1.07
5	2.6	1.05	0.71	1.86	0.29	1.28	1.12
6	3.3	1.06	0.71	1.85	0.29	1.28	1.00
7	3.9	1.03	0.66	1.79	0.34	1.28	1.04
8	4.6	1.07	0.74	1.90	0.26	1.28	1.05
9	5.2	1.01	0.64	1.79	0.36	1.29	1.10

a: Decay time, b: Fractional contribution, c: Weighted average decay time $\tau_{\text{av}} = \sum (\tau_i \times \alpha_i)$, d: Quality of fitting

3.4. Perrin calculation

During excitation, one or more analyte molecules can be statistically located within the sphere of interaction around the luminescent particles at a suitable distance to form a non-fluorescent complex, while outside this sphere the quencher does not affect the fluorescence of the sensor [1]. Perrin's static model is described by the following equation:

$$\frac{I_0}{I} = \exp(K_p[Q])$$

$$K_p = V_q N_A = \frac{4}{3} \pi R_s^3 N_A$$

Where N_A – Avogadro's number, I fluorescence intensity in the presence of a quencher, I_0 – fluorescence intensity when the concentration of the quencher is zero, R_s – the radius of the sphere.

Perrin radius values for sensors **3a,b** were calculated from the slope of the dependence $\ln(I_0/I)$ to the concentration of the quencher $[Q]$.

3.5. Stern-Volmer, Perrin, and LOD graphs for compound 3a

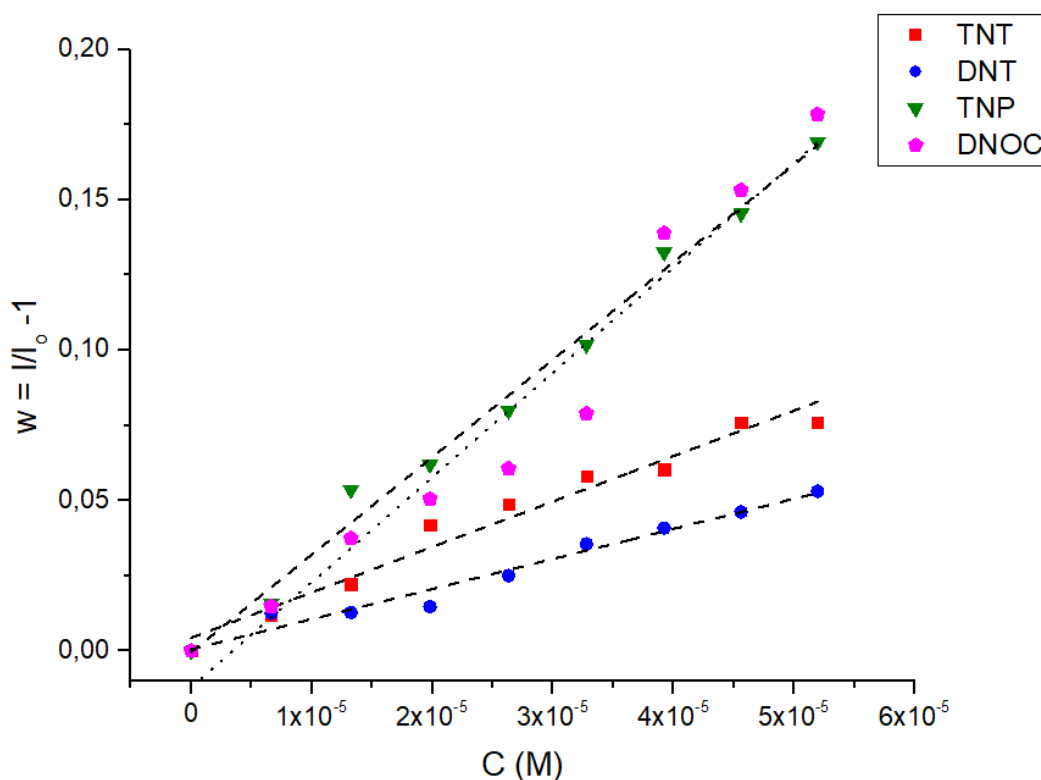


Figure S14. Stern-Volmer plots for compound **3a**. Sample preparation: for TNT: $C(\mathbf{3a}) = 5 \cdot 10^{-6}$ M, $\lambda_{em} = 460$ nm, for DNT: $C(\mathbf{3a}) = 5 \cdot 10^{-6}$ M, $\lambda_{em} = 460$ nm, for TNP: $C(\mathbf{3a}) = 1 \cdot 10^{-5}$ M, $\lambda_{em} = 420$ nm, for DNOC: $C(\mathbf{3a}) = 1 \cdot 10^{-5}$ M, $\lambda_{em} = 420$ nm.

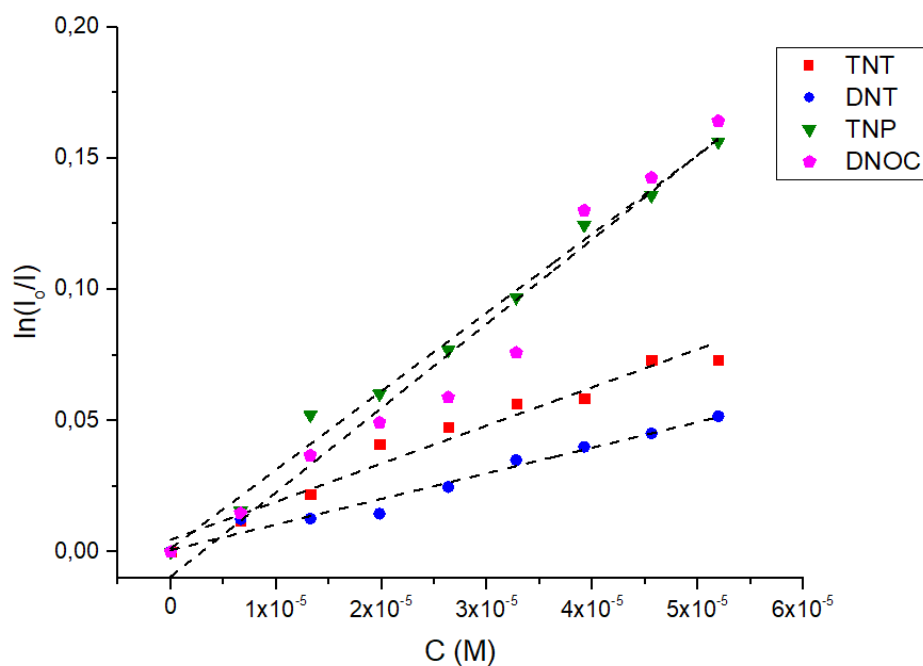


Figure S15. Perrin plots for compound **3a**. Sample preparation: for TNT: $C(\mathbf{3a}) = 5 \cdot 10^{-6}$ M, $\lambda_{em} = 460$ nm, for DNT: $C(\mathbf{3a}) = 5 \cdot 10^{-6}$ M, $\lambda_{em} = 460$ nm, for TNP: $C(\mathbf{3a}) = 1 \cdot 10^{-5}$ M, $\lambda_{em} = 420$ nm, for DNOC: $C(\mathbf{3a}) = 1 \cdot 10^{-5}$ M, $\lambda_{em} = 420$ nm.

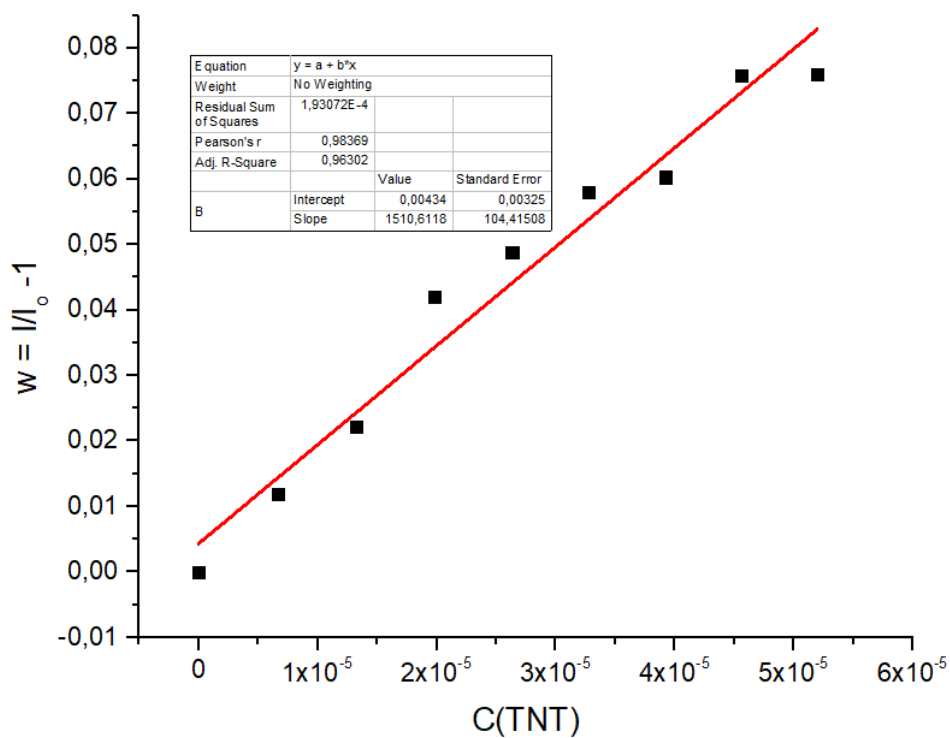


Figure S16. Stern-Volmer plot for compound **3a** in the presence of TNT. Sample preparation: $C(\mathbf{3a}) = 5 \cdot 10^{-6}$ M, $\lambda_{em} = 460$ nm

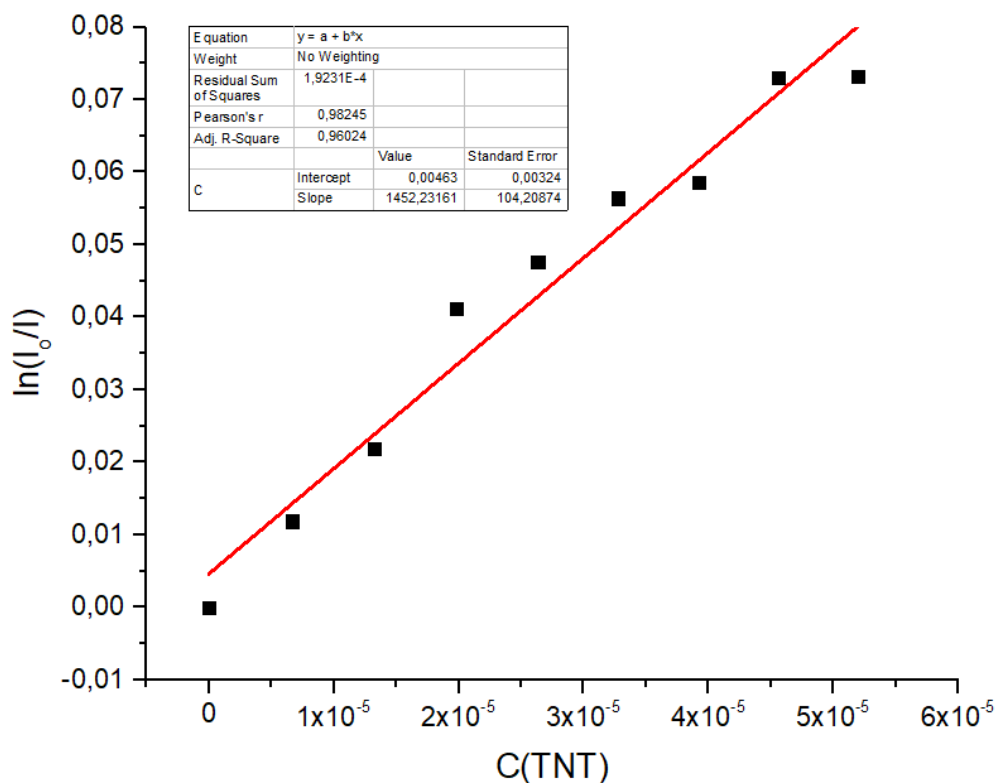


Figure S17. Perrin plot for compound **3a** in the presence of TNT. Sample preparation: $C(\mathbf{3a}) = 5 \cdot 10^{-6}$ M, $\lambda_{em} = 460$ nm

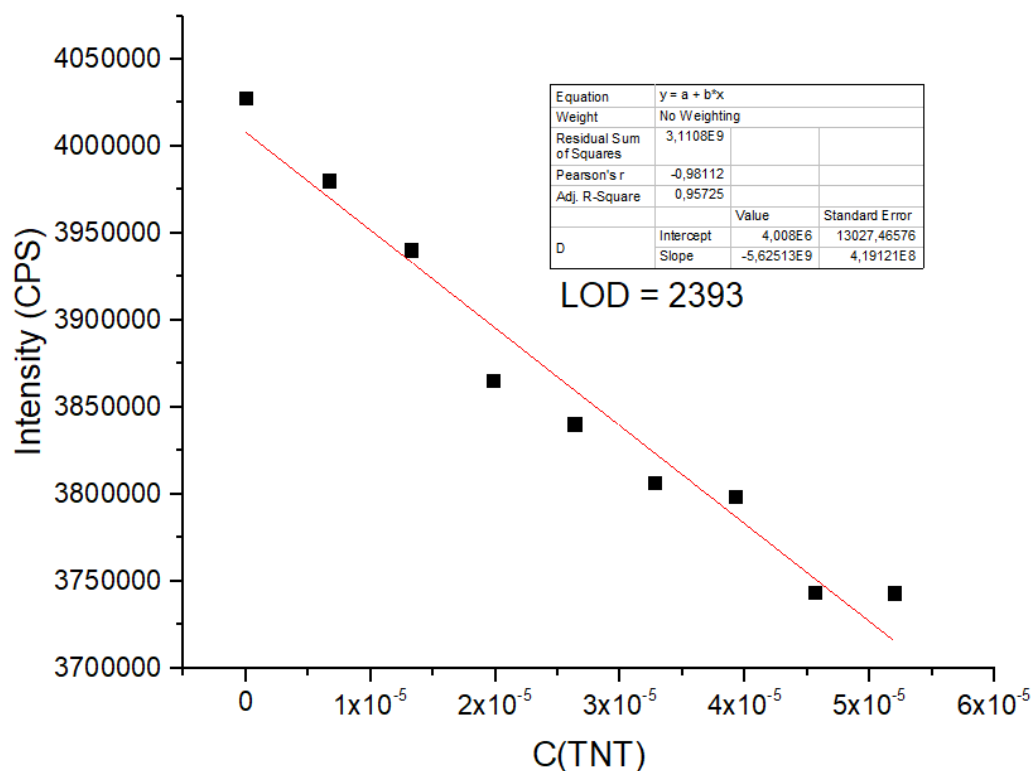


Figure S18. Limit of detection (LOD) plot for compound **3a** in the presence of TNT. Sample preparation: $C(\mathbf{3a}) = 5 \cdot 10^{-6}$ M, $\lambda_{em} = 460$ nm

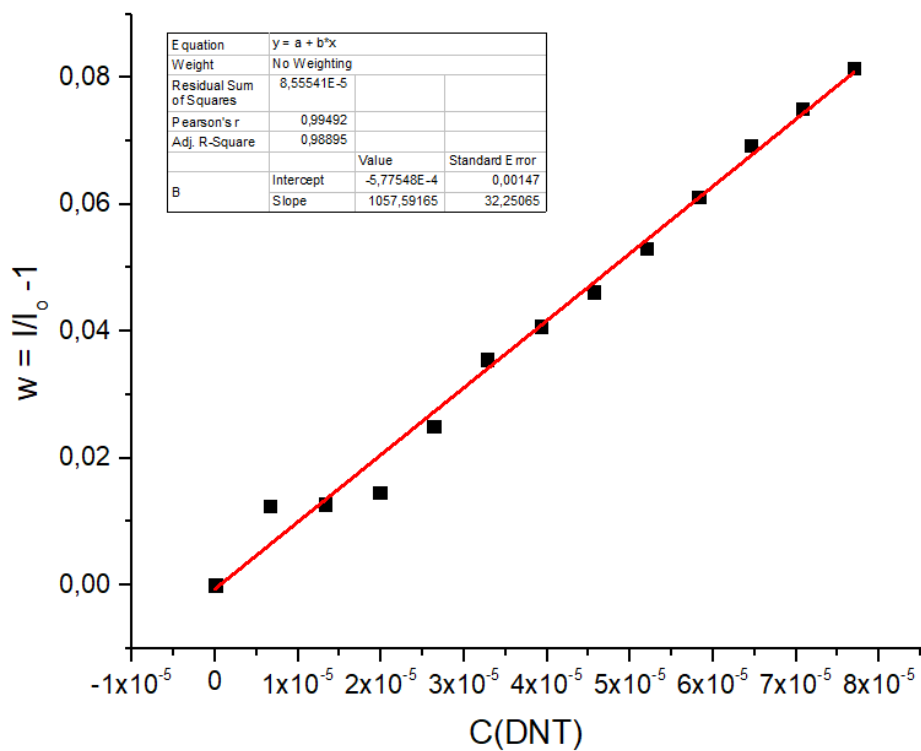


Figure S19. Stern-Volmer plot for compound **3a** in the presence of DNT. Sample preparation: $C(\mathbf{3a}) = 5 \cdot 10^{-6}$ M, $\lambda_{em} = 460$ nm

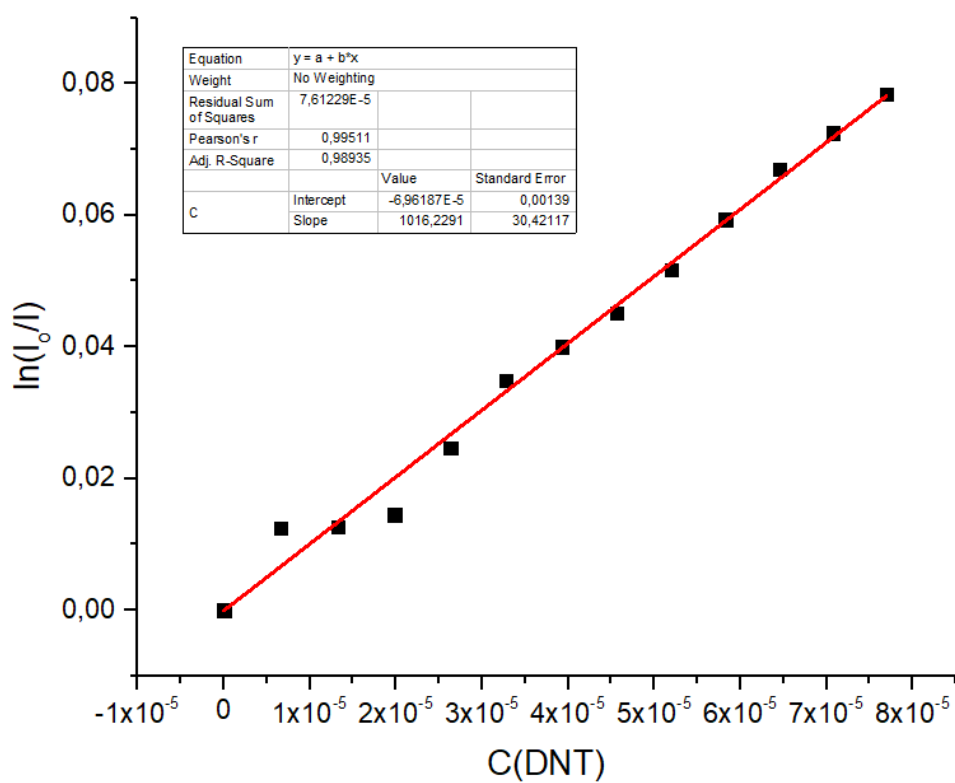


Figure S20. Perrin plot for compound **3a** in the presence of DNT. Sample preparation: $C(\mathbf{3a}) = 5 \cdot 10^{-6}$ M, $\lambda_{em} = 460$ nm

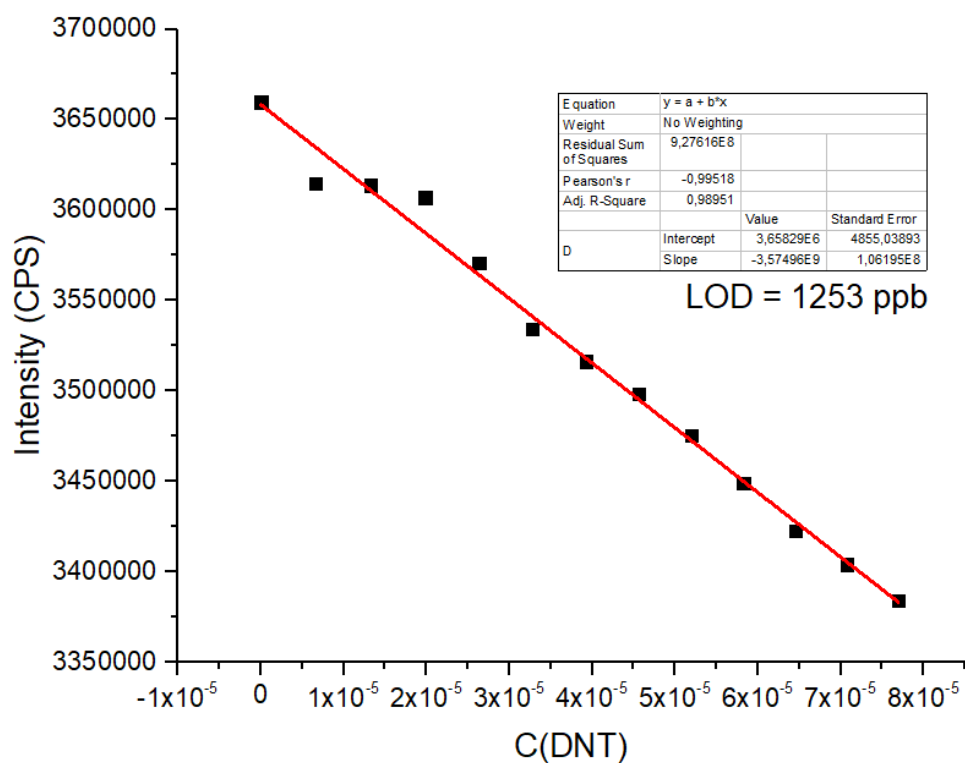


Figure S21. Limit of detection (LOD) plot for compound **3a** in the presence of DNT. Sample preparation: $C(\mathbf{3a}) = 5 \cdot 10^{-6}$ M, $\lambda_{em} = 460$ nm

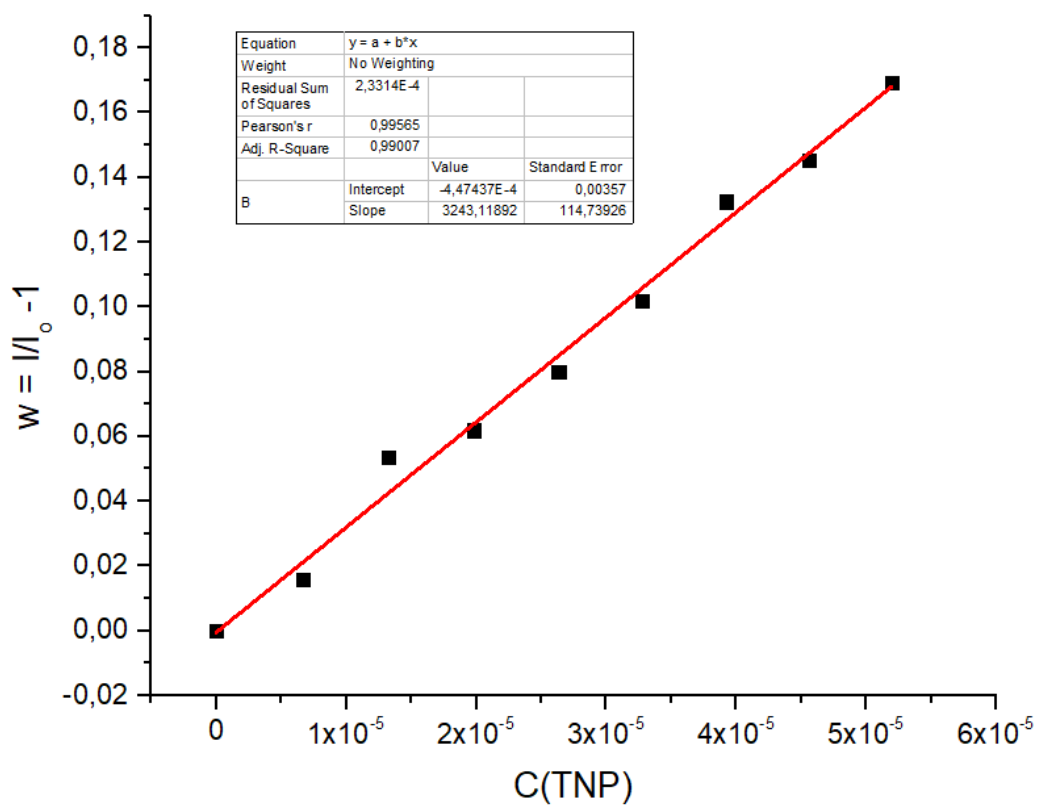


Figure S22. Stern-Volmer plot for compound **3a** in the presence of TNP. Sample preparation: $C(\mathbf{3a}) = 1 \cdot 10^{-5}$ M, $\lambda_{em} = 420$ nm

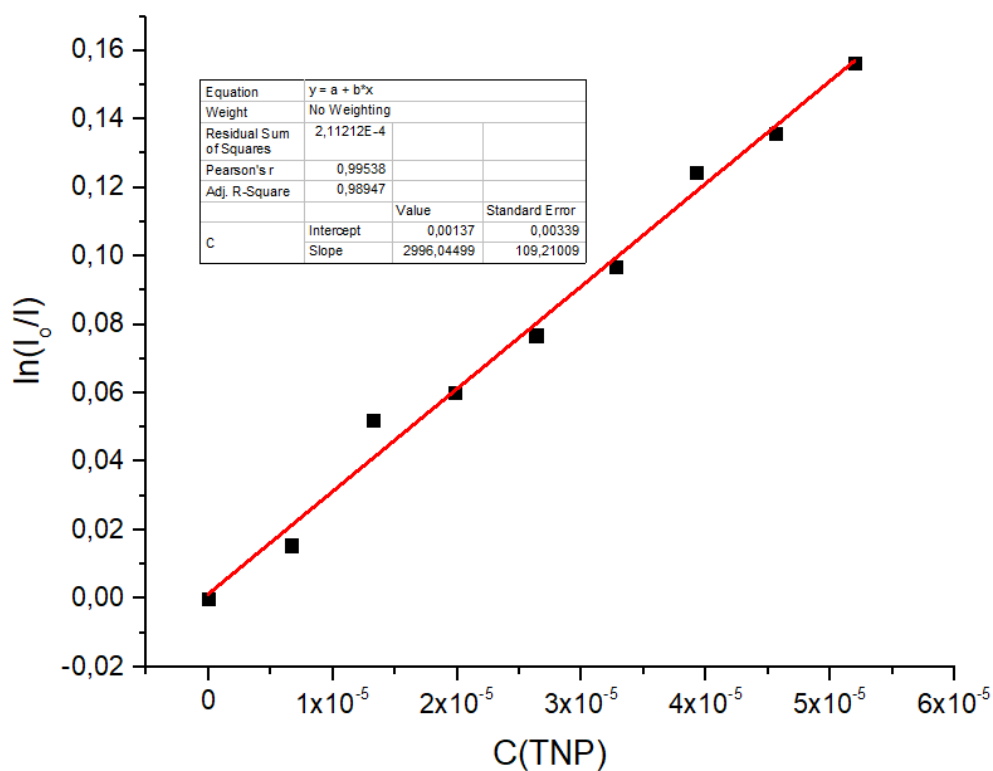


Figure S23. Perrin plot for compound **3a** in the presence of TNP. Sample preparation: $C(\mathbf{3a}) = 1 \cdot 10^{-5}$ M, $\lambda_{em} = 420$ nm

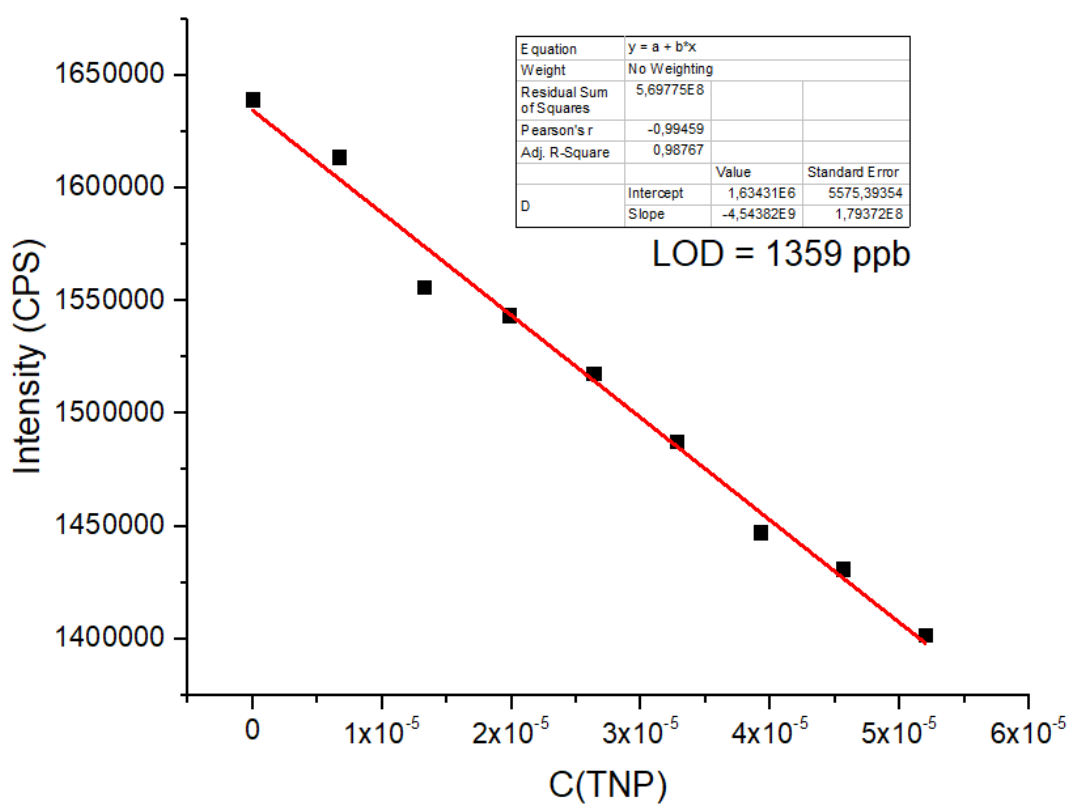


Figure S24. Limit of detection (LOD) plot for compound **3a** in the presence of TNP. Sample preparation: $C(\mathbf{3a}) = 1 \cdot 10^{-5}$ M, $\lambda_{em} = 420$ nm

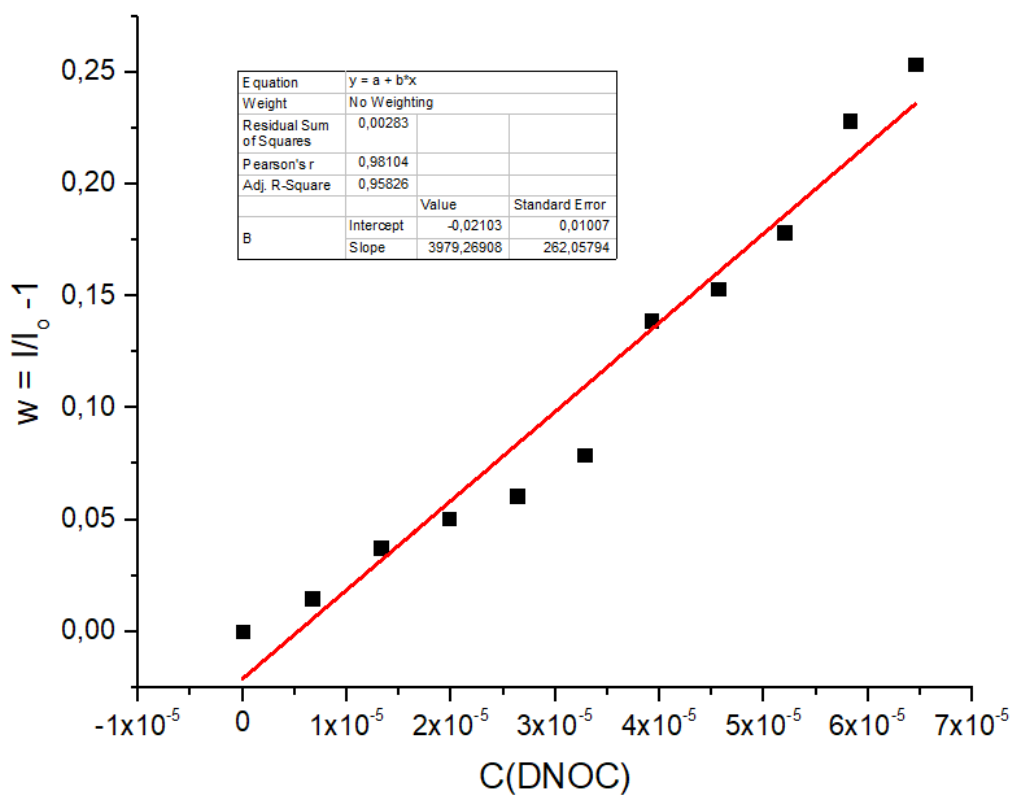


Figure S25. Stern-Volmer plot for compound **3a** in the presence of DNOC. Sample preparation: $C(\mathbf{3a}) = 1 \cdot 10^{-5}$ M, $\lambda_{em} = 420$ nm

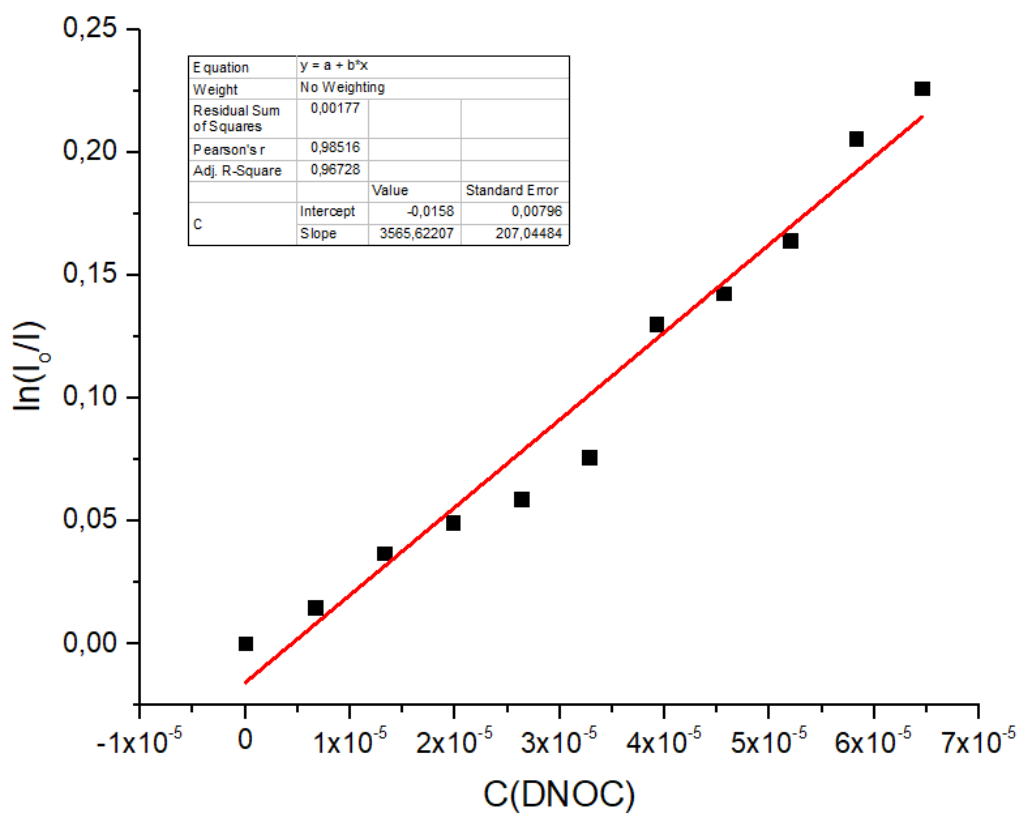


Figure S26. Perrin plot for compound **3a** in the presence of DNOC. Sample preparation: $C(\mathbf{3a}) = 1 \cdot 10^{-5}$ M, $\lambda_{em} = 420$ nm

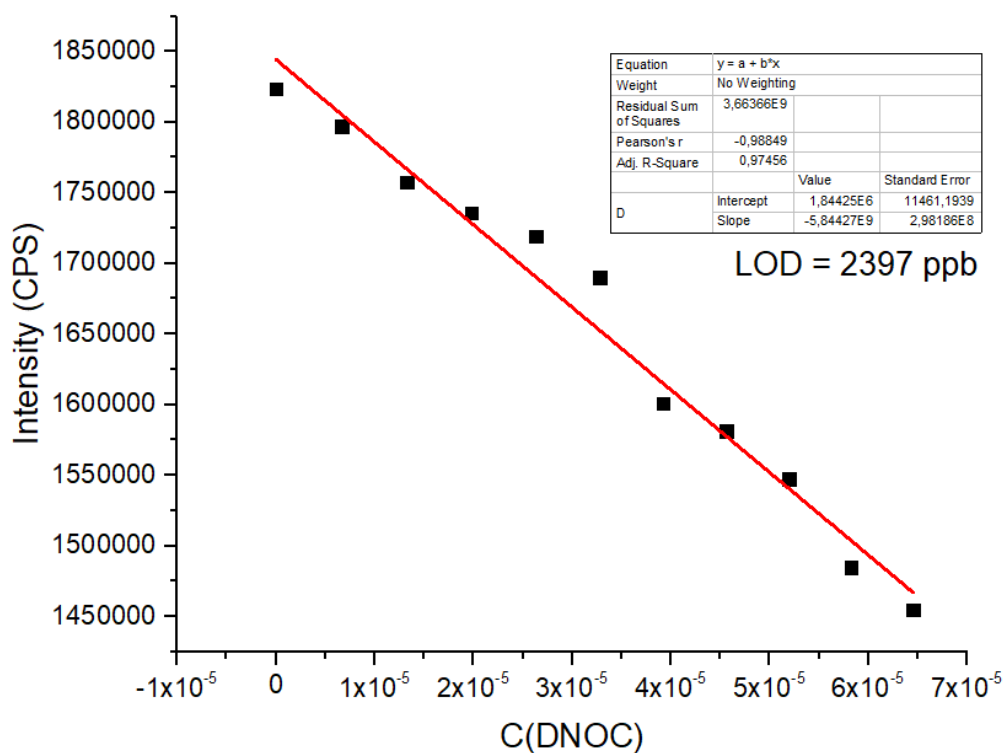


Figure S27. Limit of detection (LOD) plot for compound **3a** in the presence of TNP. Sample preparation: $C(\mathbf{3a}) = 1 \cdot 10^{-5}$ M, $\lambda_{em} = 420$ nm

3.6. Stern-Volmer, Perrin and LOD graphs for compounds **3b**

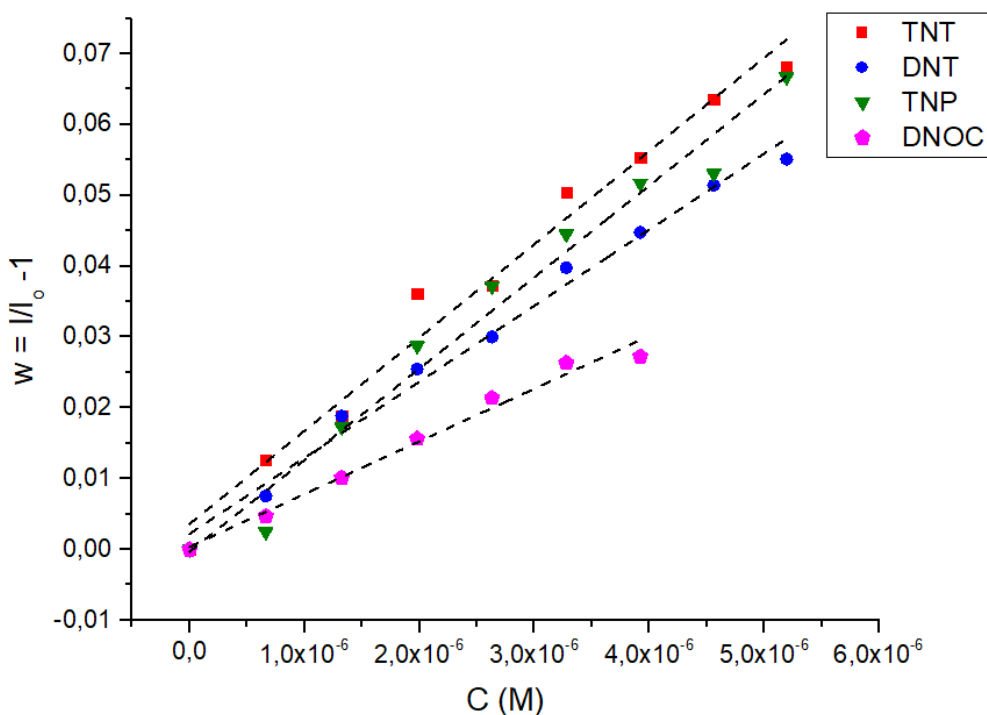


Figure S28. Stern-Volmer plots for compound **3b**. Sample preparation: for TNT: $C(\mathbf{3b}) = 5 \cdot 10^{-6}$ M, $\lambda_{em} = 465$ nm, for DNT: $C(\mathbf{3b}) = 5 \cdot 10^{-6}$ M, $\lambda_{em} = 465$ nm, for TNP: $C(\mathbf{3b}) = 3 \cdot 10^{-6}$ M, $\lambda_{em} = 470$ nm, for DNOC: $C(\mathbf{3b}) = 3 \cdot 10^{-6}$ M, $\lambda_{em} = 470$ nm.

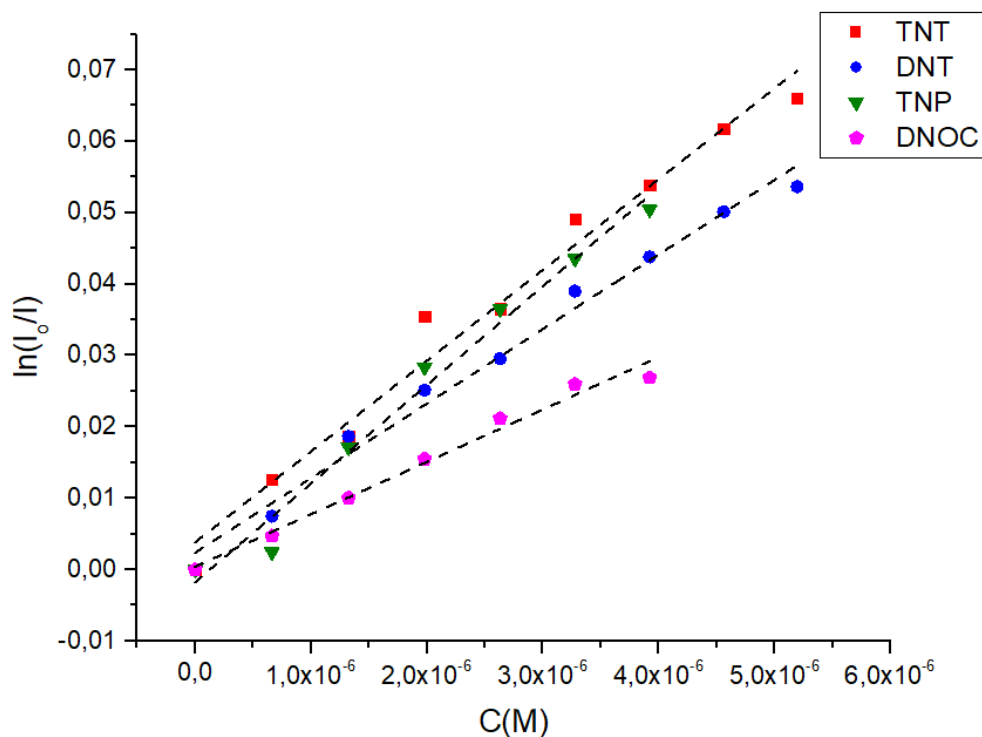


Figure S29. Perrin plots for compound **3b**. Sample preparation: for TNT: $C(\mathbf{3b}) = 5 \cdot 10^{-6}$ M, $\lambda_{em} = 465$ nm, for DNT: $C(\mathbf{3b}) = 5 \cdot 10^{-6}$ M, $\lambda_{em} = 465$ nm, for TNP: $C(\mathbf{3a}) = 3 \cdot 10^{-6}$ M, $\lambda_{em} = 470$ nm, for DNOC: $C(\mathbf{3b}) = 3 \cdot 10^{-6}$ M, $\lambda_{em} = 470$ nm.

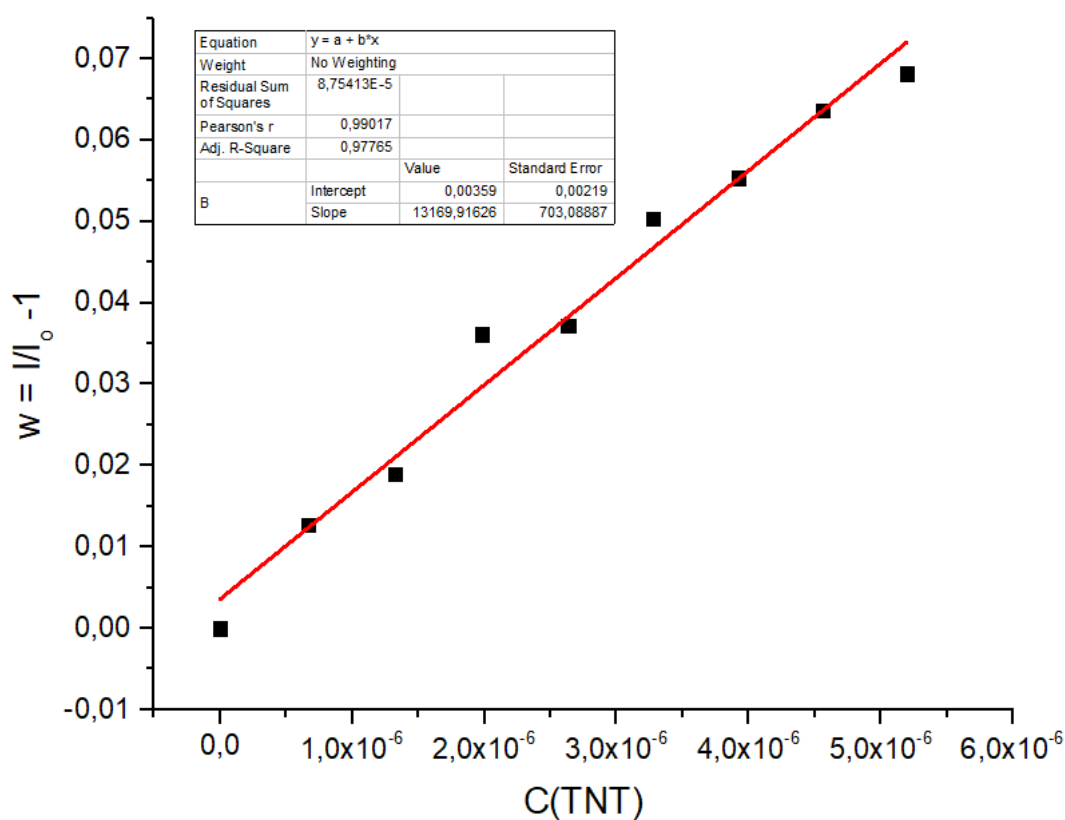


Figure S30. Stern-Volmer plot for compound **3b** in the presence of TNT. Sample preparation: $C(\mathbf{3b}) = 5 \cdot 10^{-6}$ M, $\lambda_{em} = 465$ nm

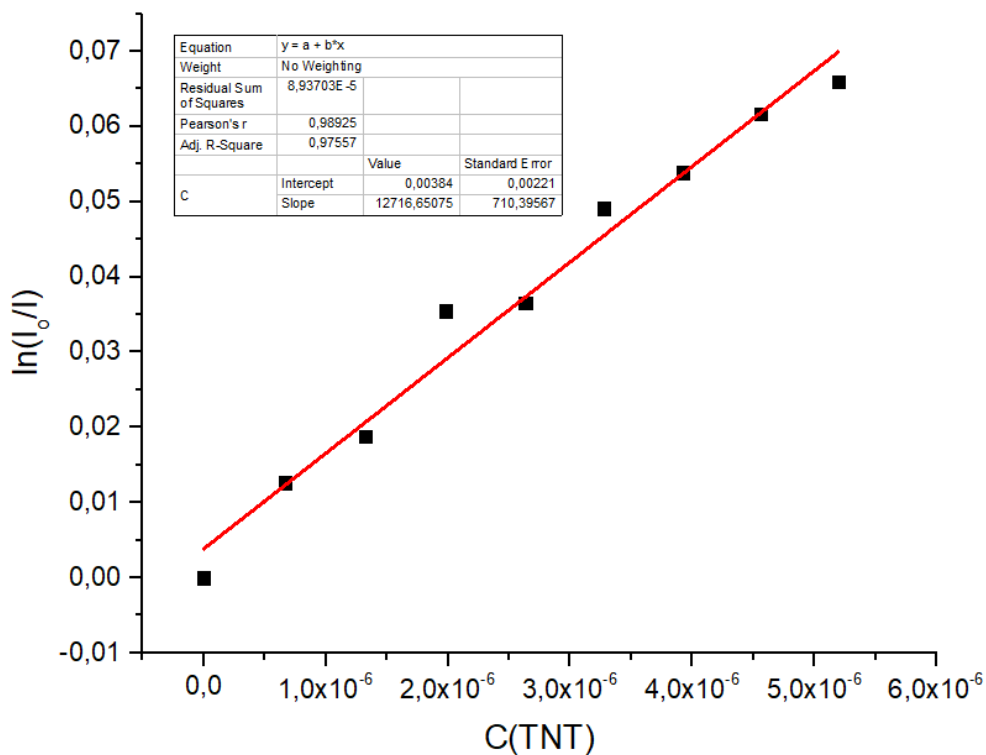


Figure S31. Stern-Volmer plot for compound **3b** in the presence of TNT. Sample preparation: $C(\mathbf{3b}) = 5 \cdot 10^{-6} \text{ M}$, $\lambda_{em} = 465 \text{ nm}$

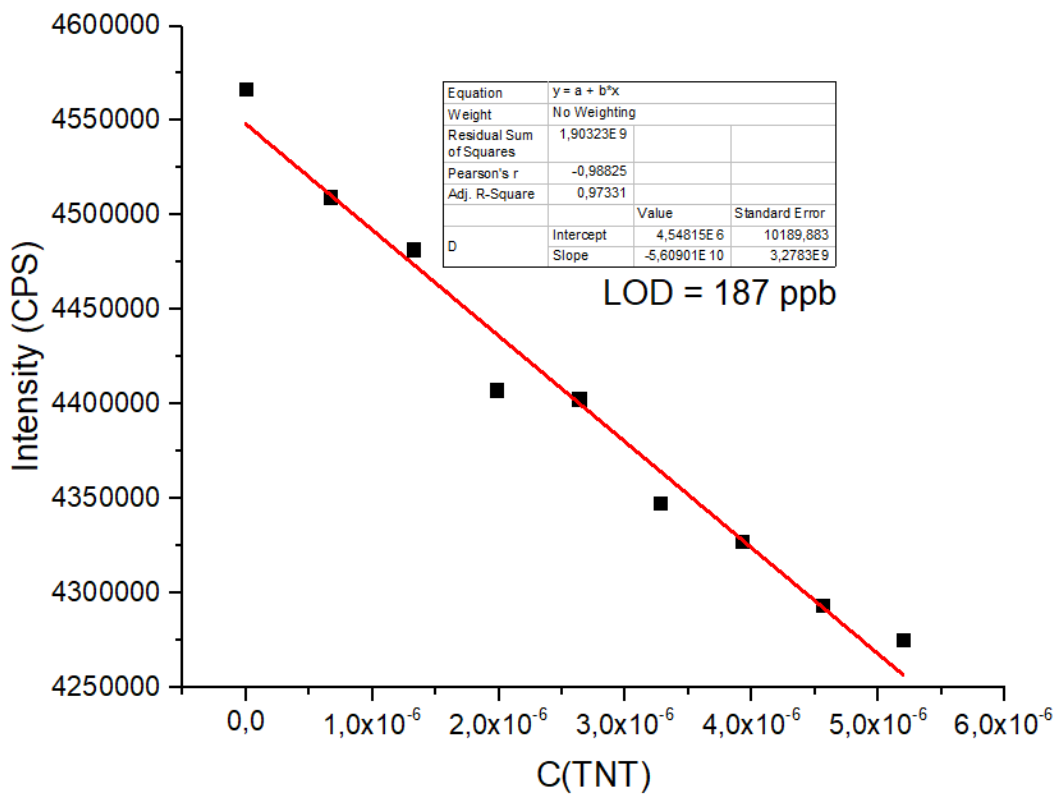


Figure S32. Limit of detection (LOD) plot for compound **3b** in the presence of TNT. Sample preparation: $C(\mathbf{3b}) = 5 \cdot 10^{-6} \text{ M}$, $\lambda_{em} = 465 \text{ nm}$

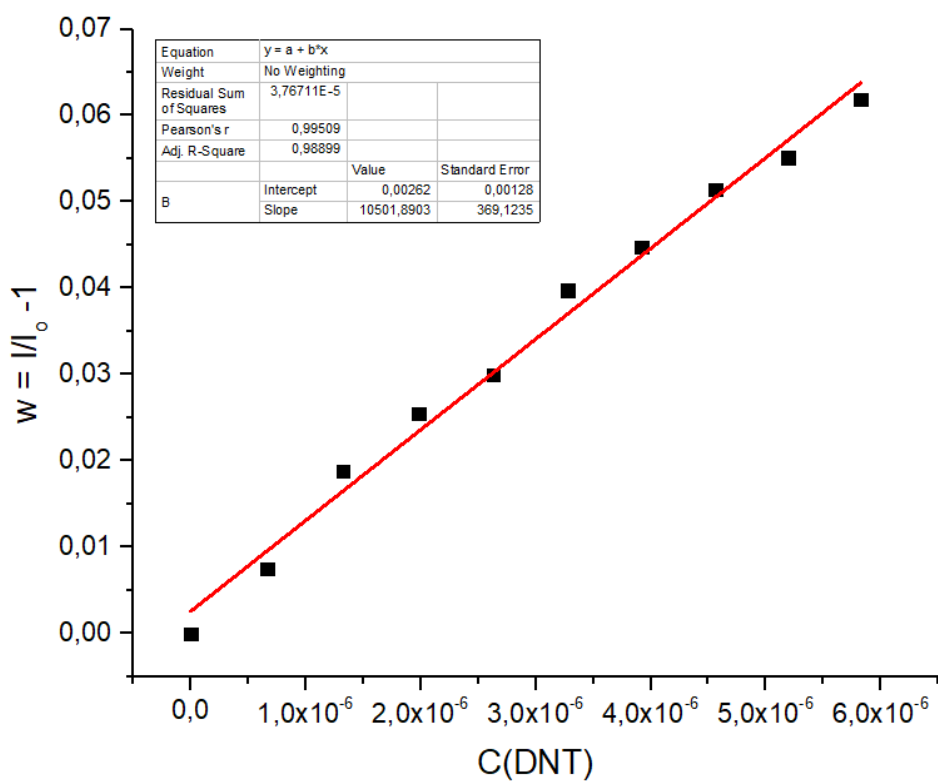


Figure S33. Stern-Volmer plot for compound **3b** in the presence of DNT. Sample preparation: $C(\mathbf{3b}) = 5 \cdot 10^{-6} \text{ M}$, $\lambda_{\text{em}} = 465 \text{ nm}$

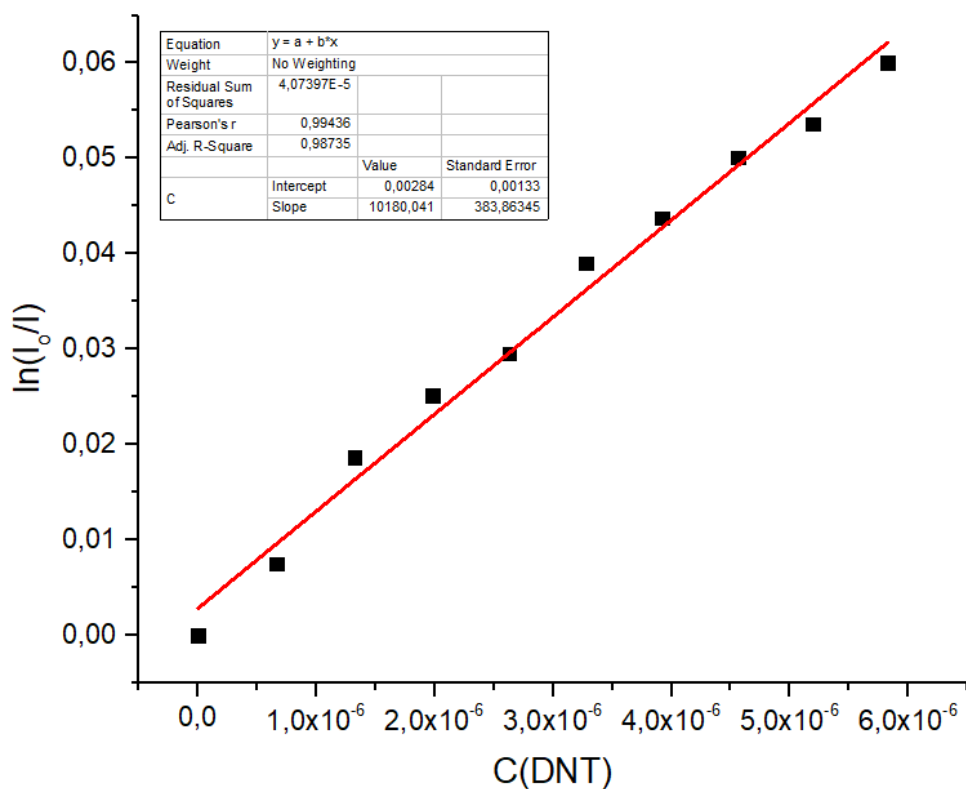


Figure S34. Perrin plot for compound **3b** in the presence of DNT. Sample preparation: $C(\mathbf{3b}) = 5 \cdot 10^{-6} \text{ M}$, $\lambda_{\text{em}} = 465 \text{ nm}$

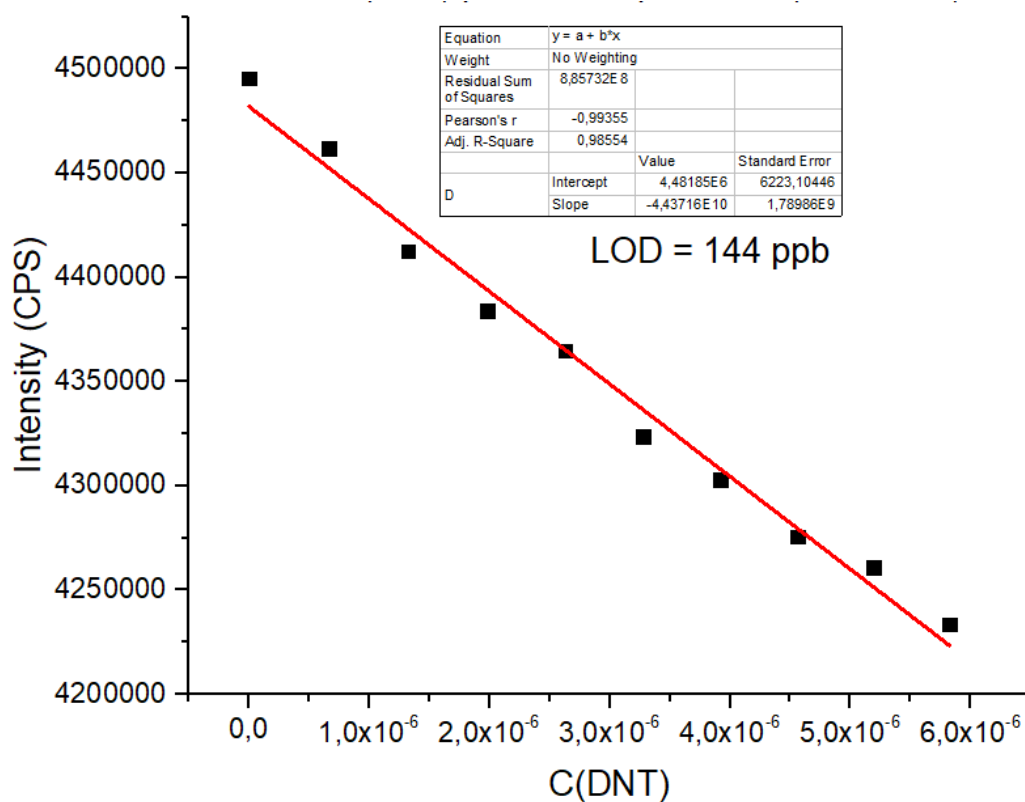


Figure S35. Limit of detection (LOD) plot for compound **3b** in the presence of DNT. Sample preparation: $C(\mathbf{3b}) = 5 \cdot 10^{-6}$ M, $\lambda_{em} = 465$ nm

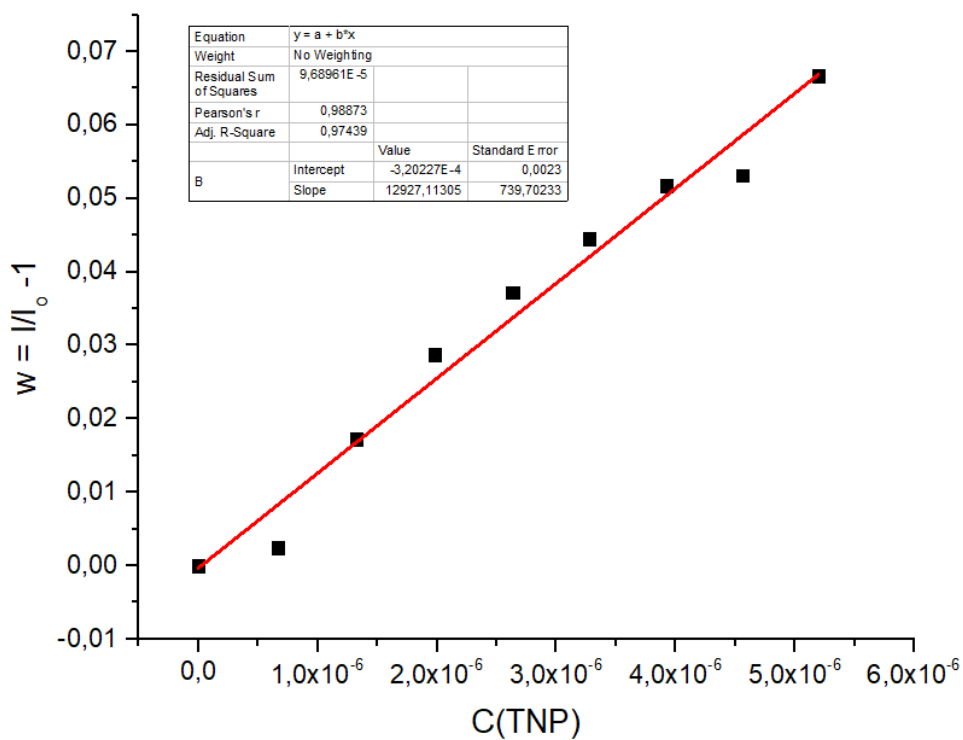


Figure S36. Stern-Volmer plot for compound **3b** in the presence of TNP. Sample preparation: $C(\mathbf{3b}) = 3 \cdot 10^{-6}$ M, $\lambda_{em} = 470$ nm

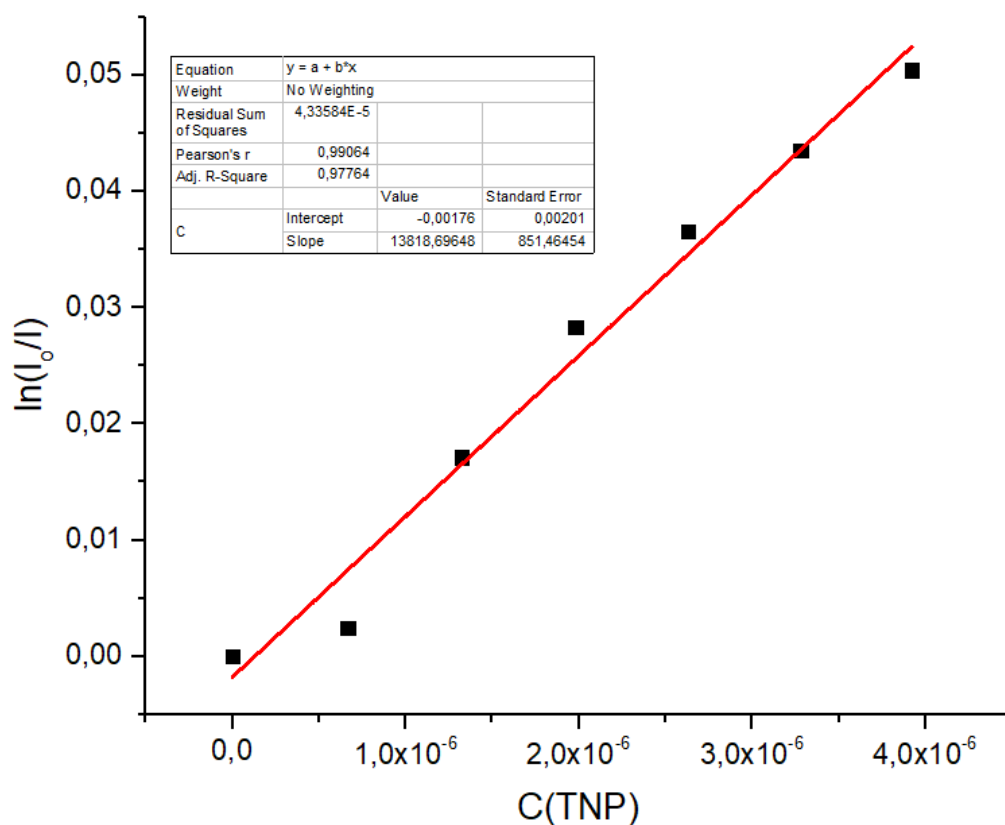


Figure S37. Perrin plot for compound **3b** in the presence of TNP. Sample preparation: $C(\mathbf{3b}) = 3 \cdot 10^{-6}$ M, $\lambda_{em} = 470$ nm

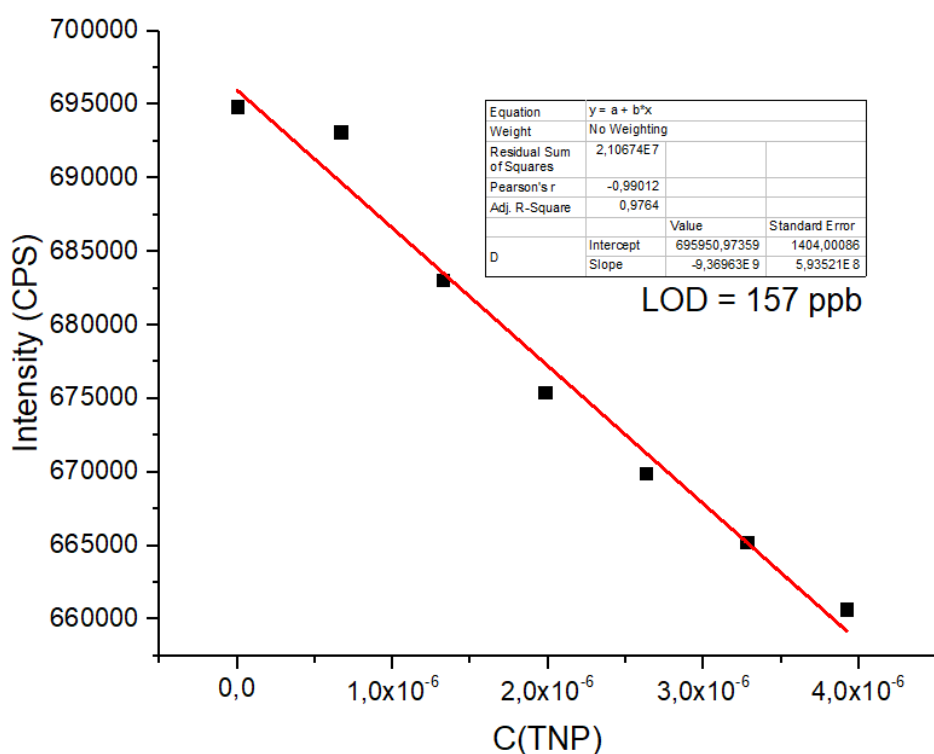


Figure S38. Limit of detection (LOD) plot for compound **3b** in the presence of TNP. Sample preparation: $C(\mathbf{3b}) = 3 \cdot 10^{-6}$ M, $\lambda_{em} = 470$ nm

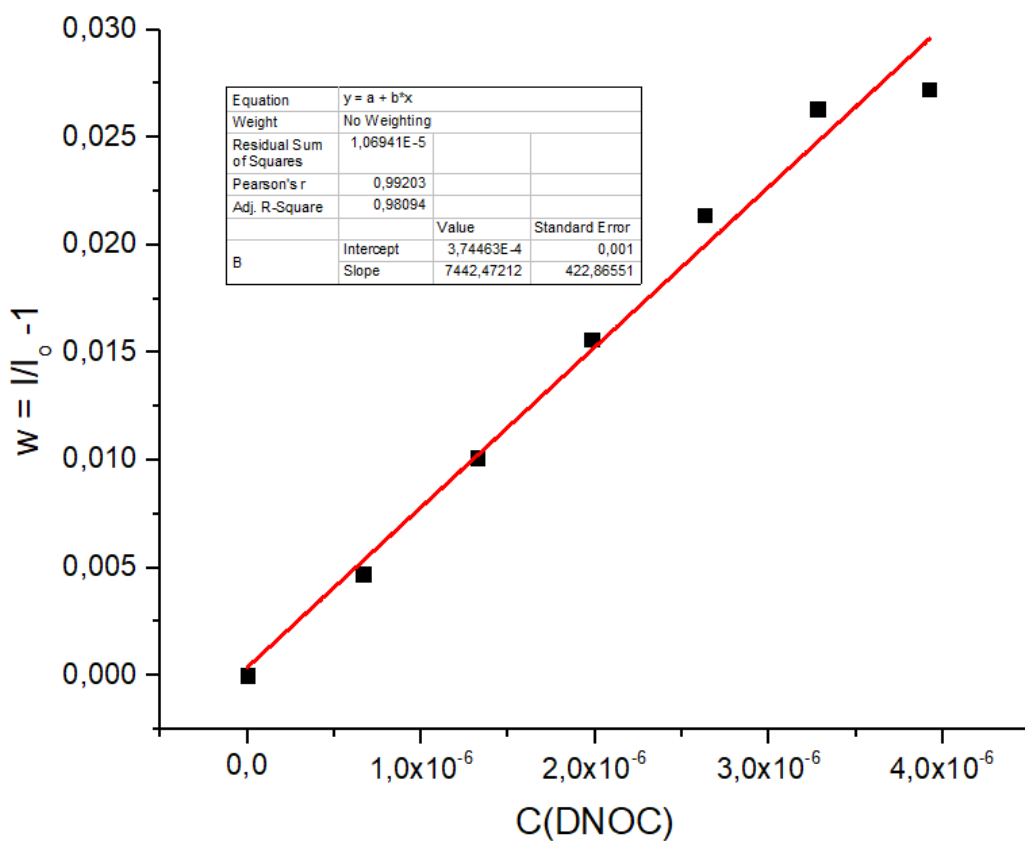


Figure S39. Stern-Volmer plot for compound **3b** in the presence of DNOC. Sample preparation: $C(\mathbf{3b}) = 3 \cdot 10^{-6}$ M, $\lambda_{em} = 470$ nm

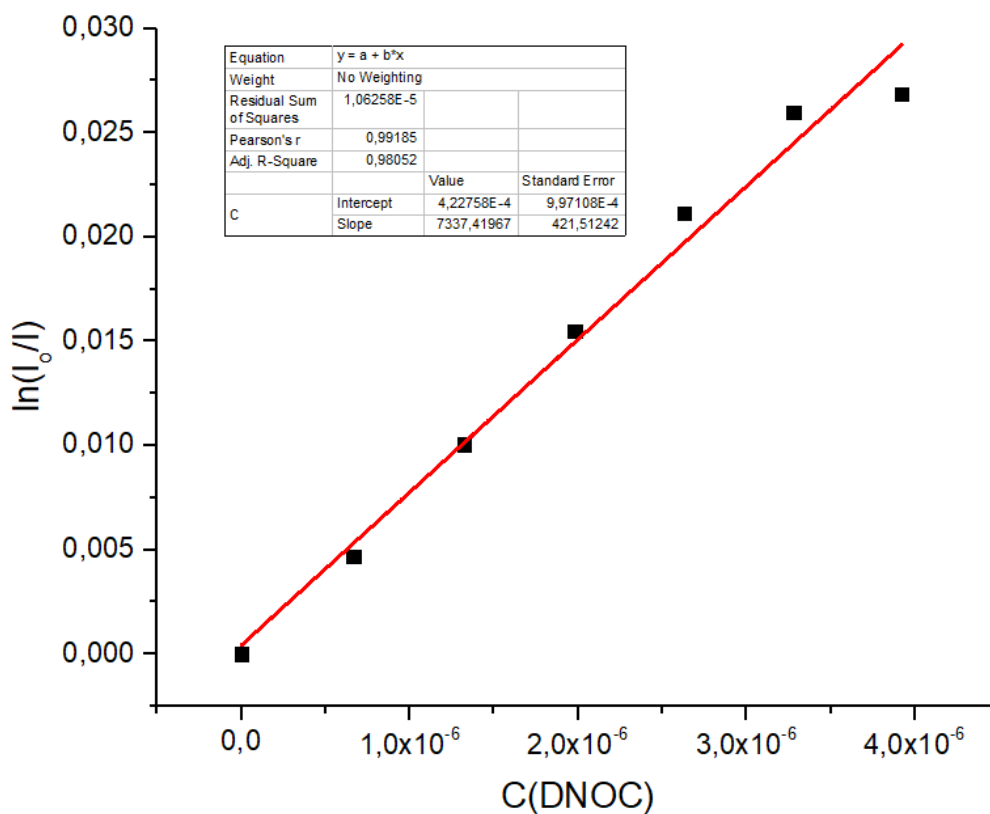


Figure S40. Perrin plot for compound **3b** in the presence of DNT. Sample preparation: $C(\mathbf{3b}) = 3 \cdot 10^{-6}$ M, $\lambda_{em} = 470$ nm

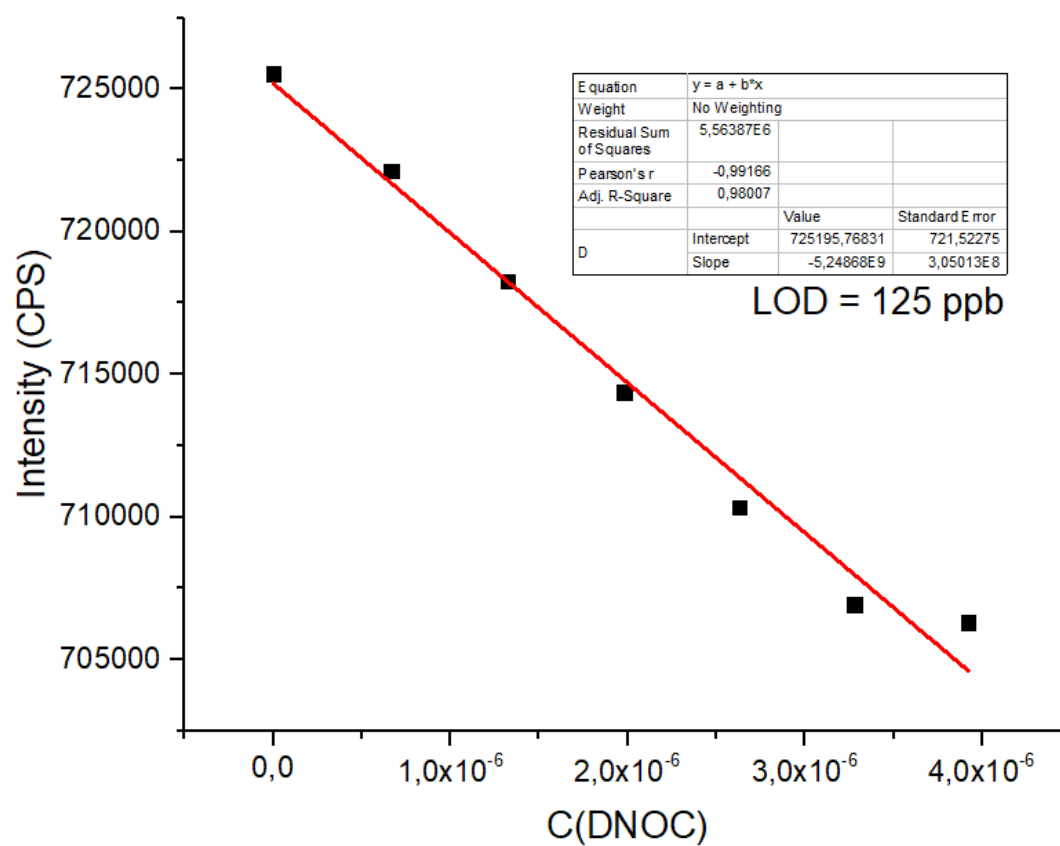


Figure S41. Limit of detection (LOD) plot for compound **3b** in the presence of DNOC. Sample preparation: $C(\mathbf{3b}) = 3 \cdot 10^{-6}$ M, $\lambda_{em} = 470$ nm

4. DFT calculations

Table S3. Calculated energy of HOMO/LUMO (HOMO-1/LUMO+1), energy gaps and dipole moments of **3a**, **b**, TNT, DNT, TNP, DNOC based on B3LYP/6-311G* functional (gas phase)

	3a	3b	TNT	DNT	TNP	DNOC
$E_{\text{LUMO}+1}$ (eV)	-1,96494	-2,03269	-3,75844	-3,18455	-3,78456	-3,08686
E_{LUMO} (eV)	-2,89557	-2,91298	-3,91382	-3,39625	-4,31464	-3,41122
E_{HOMO} (eV)	-6,26053	-6,04882	-8,83962	-8,43771	-8,61731	-7,7128
$E_{\text{HOMO}-1}$ (eV)	-7,22871	-6,77945	-8,96643	-8,47363	-9,11119	-8,36805
ΔE_{0-0} (eV)	3,36496	3,13584	4,92581	5,04146	4,30267	4,30158
μ (D)	2,37183	3,15009	1,67874	5,24597	1,62381	5,27665

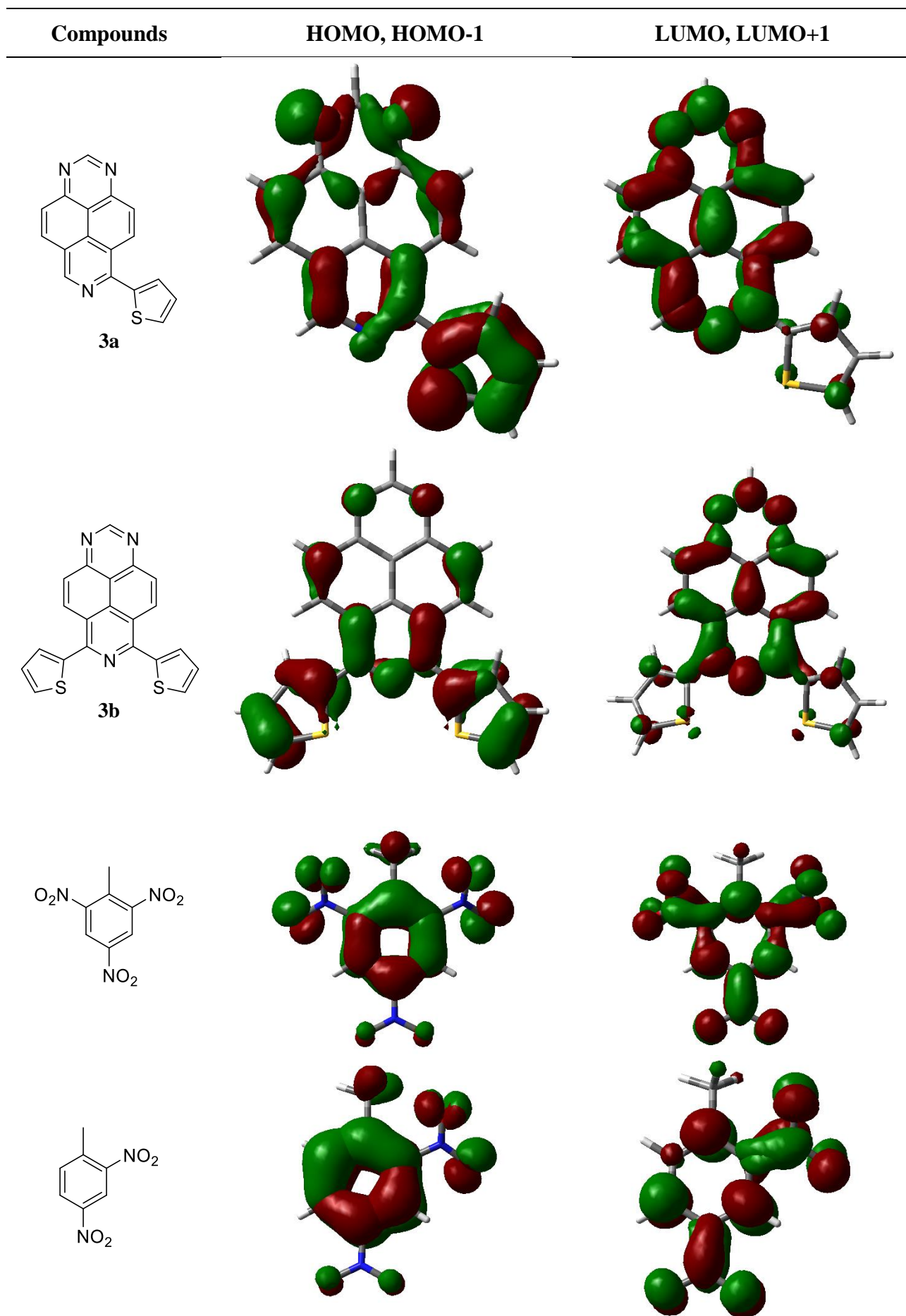
Table S4. Mulliken population analysis for compounds **3a**,**b**

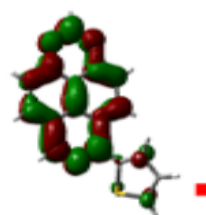
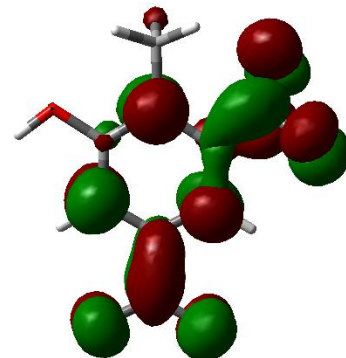
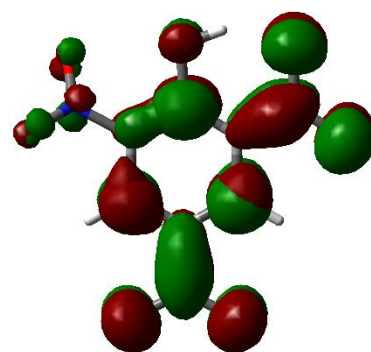
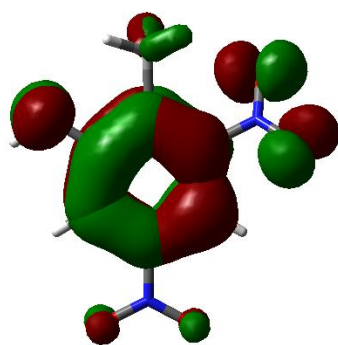
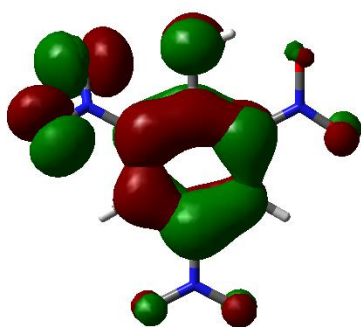
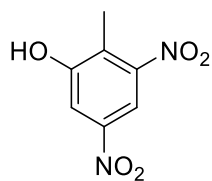
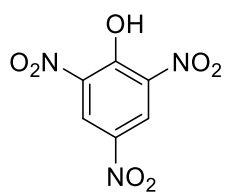
3a		3b		
1	C	0,11836	1 C	0,240702
2	C	0,18727	2 C	0,000555
3	C	1,19431	3 C	0,142453
4	C	-0,32877	4 C	0,000554
5	C	-0,81228	5 C	-0,38997
6	C	0,88242	6 C	0,902025
7	C	1,04281	7 C	0,786385
8	C	-1,0733	8 C	-0,71895
9	C	-1,33585	9 C	-0,67304
10	C	-0,25753	10 C	-0,67304
11	C	0,37942	11 C	0,786385
12	C	-0,52038	12 C	-0,71895
13	C	-0,77422	13 C	-0,38997
14	H	0,14034	17 C	0,184405
15	H	0,13272	18 C	0,405328
16	H	0,1399	19 S	-0,21041
17	H	0,12039	20 C	-0,29426
18	C	0,37407	22 C	0,134119
19	C	0,18603	27 N	-0,08454
20	S	-0,14005	28 N	-0,08454
21	C	-0,39416	29 N	0,435592
22	H	0,13991	30 C	0,184403
23	C	-0,06297	31 C	0,405326
24	H	0,13302	32 S	-0,21041
25	H	0,16184	33 C	-0,29426
26	H	0,15846	35 C	0,134119
27	H	0,13835		
28	N	-0,0651		
29	N	-0,0718		
30	N	0,20679		

Table S5. Mulliken population analysis for nitroaromatics

TNT			DNT			TNP			DNOC		
1	C	-0,36182	1	C	-1,30971	1	C	0,679784	1	C	-1,96219
2	C	1,163007	2	C	1,986392	2	C	-0,90973	2	C	2,563448
3	C	-0,30904	3	C	0,37256	3	C	-0,28179	3	C	0,427872
4	C	-0,36167	4	C	-1,55838	4	C	0,311785	4	C	-1,79109
5	C	-0,30914	5	C	0,360889	5	C	-0,06581	5	C	0,723928
6	C	0,250287	6	C	-0,21282	6	C	0,358547	6	C	-0,39714
7	H	0,196867	7	H	0,17157	7	H	0,207142	7	H	0,188766
8	N	-0,25866	8	N	-0,24888	8	N	-0,27643	8	N	-0,24871
9	O	0,024431	9	O	0,004667	9	O	0,029623	9	O	0,021042
10	O	0,024437	10	O	0,016608	10	O	0,025616	10	O	0,001125
11	N	-0,22672	11	N	-0,24443	11	N	-0,29048	11	N	-0,24738
12	O	0,030399	12	O	0,009705	12	O	-0,02744	12	O	0,024565
13	O	0,048047	13	O	0,02946	13	O	0,068209	13	O	0,039005
14	N	-0,22674	14	C	-0,23283	14	N	-0,24793	14	C	-0,0631
15	O	0,030378	15	H	0,143492	15	O	0,054393	15	H	0,163392
16	O	0,048026	16	H	0,172333	16	O	0,026797	16	H	0,16635
17	C	-0,51143	17	H	0,199797	17	H	0,200993	17	H	0,197735
18	H	0,165666	18	H	0,197472	18	O	-0,1639	18	H	0,151161
19	H	0,165671	19	H	0,1421	19	H	0,300615	19	O	-0,22617
20	H	0,221127							20	H	0,267384
21	H	0,196878									

5. Molecular orbitals images





LUMO

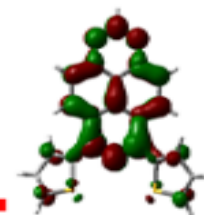
-2.90

$\Delta E = 3.36$

HOMO

-6.26

Sensor 3a



-2.91

$\Delta E = 3.14$

-6.05

Sensor 3b

Figure S42. DFT calculated of energy gaps for sensors **3a,b**

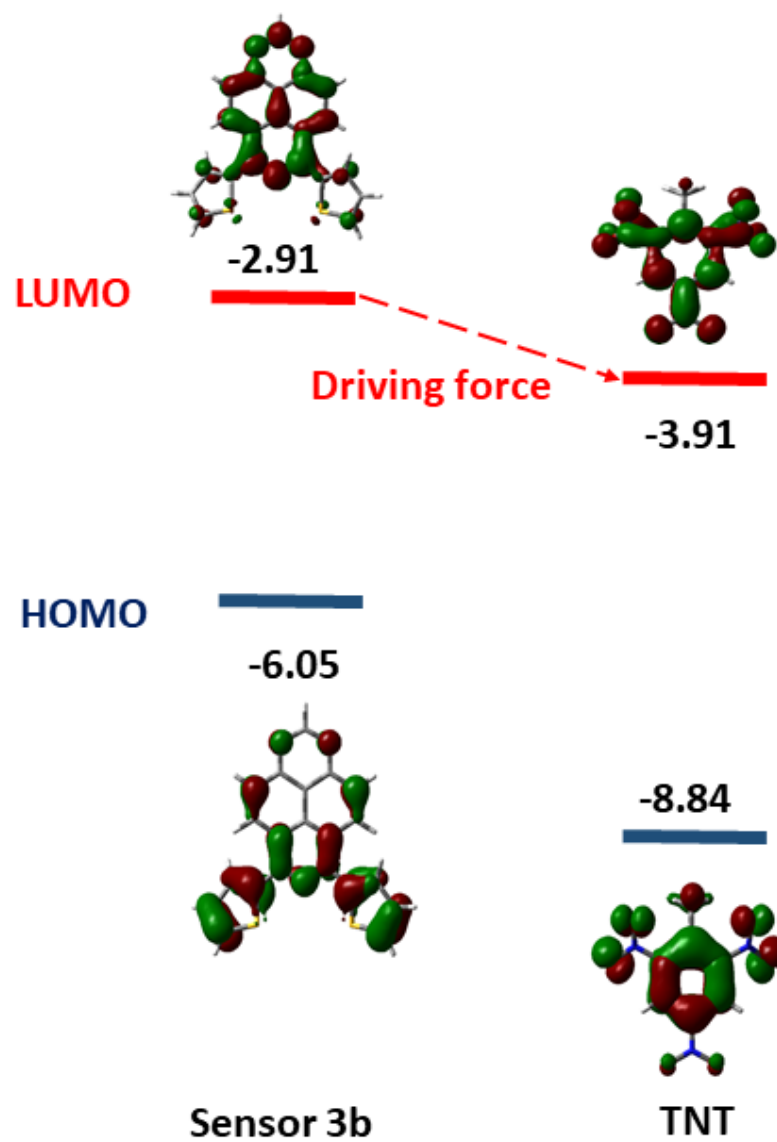
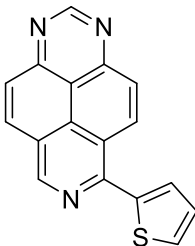
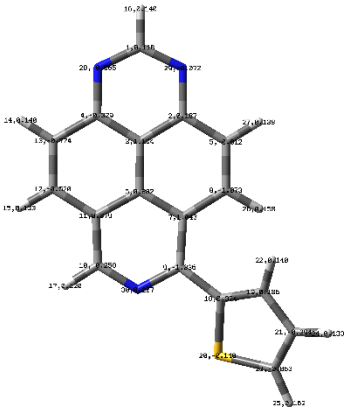
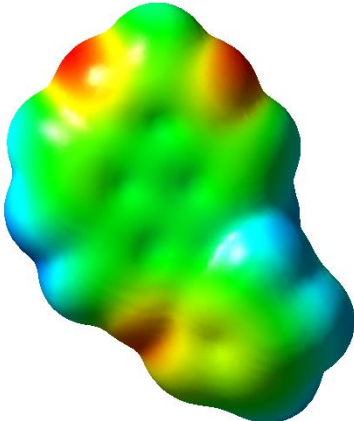
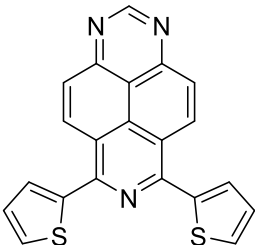
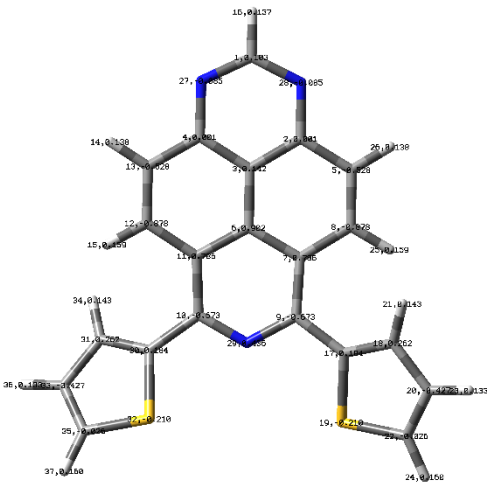
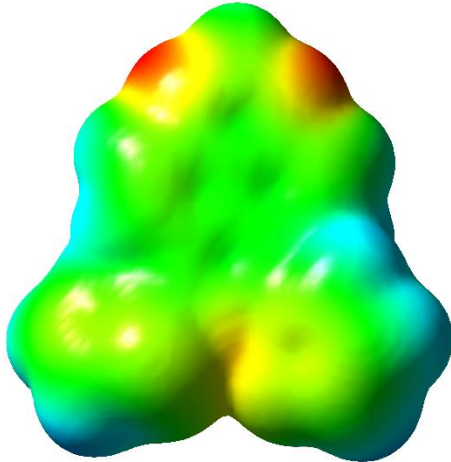
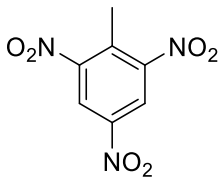
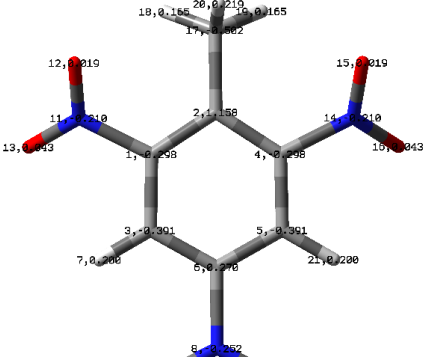
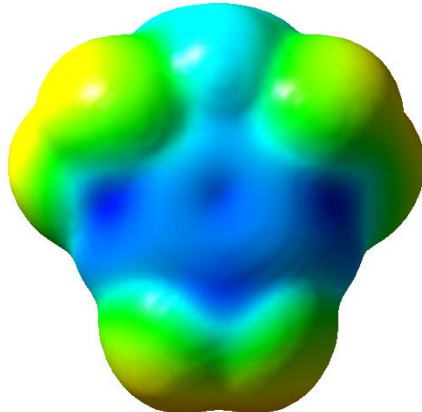
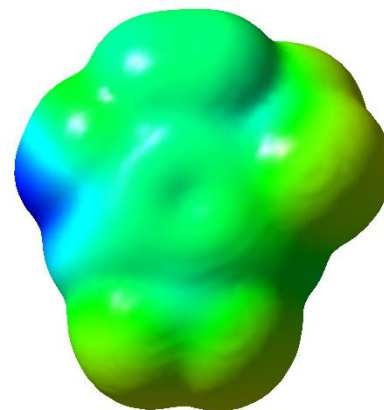
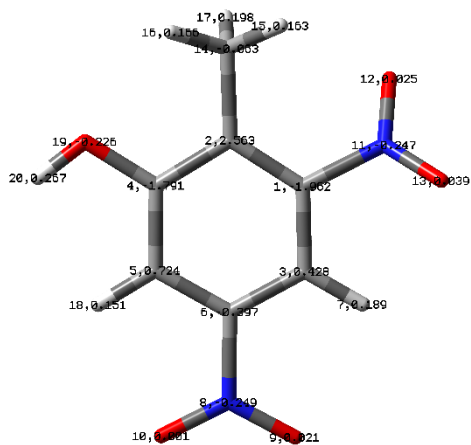
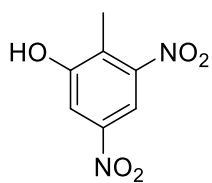
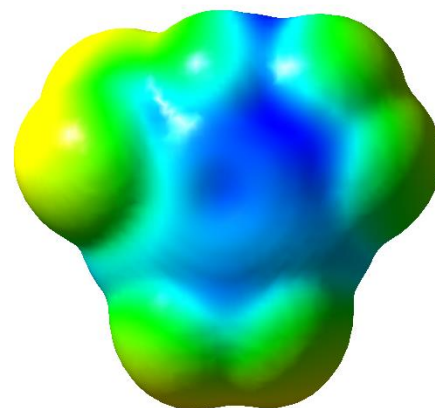
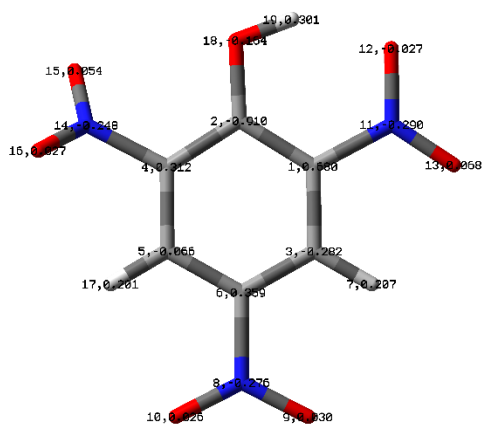
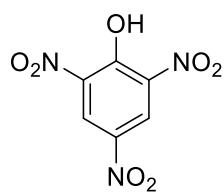
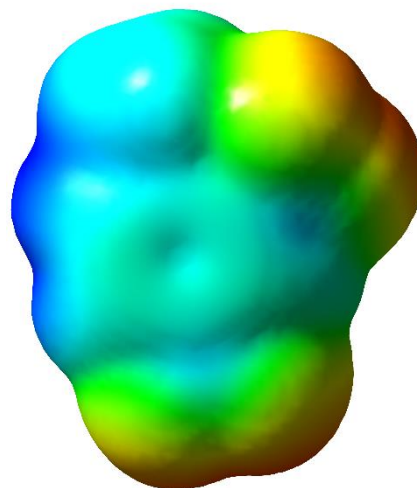
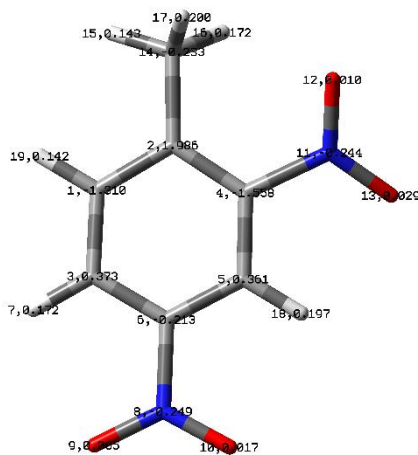
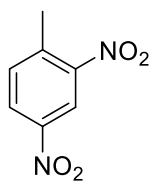


Figure S43. DFT calculated energy of HOMO/LUMO of sensors **3a, b**

6. The molecular electronic potential diagrams

Compounds	The molecular electronic potential diagrams	The molecular electronic potential diagrams
 <p data-bbox="336 613 373 645">3a</p>		
 <p data-bbox="336 1106 373 1137">3b</p>		
		



References

1. D. Genovese, M. Cingolani, E. Rampazzo, L. Prodi, N. Zaccheroni, *Chem. Soc. Rev.*, 2021, **50**, 8414-8427.